Structural Response of Masonry Infilled Timber Frames to Flood and Wind Driven Rain Exposure

Victoria Stephenson, Ph.D[1]; Dina D'Ayala, Ph.D[2]

[1] Research Associate, CEGE, UCL, Chadwick Building, Gower Street, London, WC1E 6BT, victoria.stephenson.12@ucl.ac.uk

[2] Professor of Structural Engineering, CEGE, UCL, Chadwick Building, Gower Street, London, WC1E 6BT, d.dayala@ucl.ac.uk

Corresponding Author: victoria.stephenson.12@ucl.ac.uk

Abstract

In the current changing climate historic timber frame buildings are exposed to ever more severe and frequent extreme weather conditions such as floods and wind driven rainstorms. These structures are especially vulnerable to moisture ingress and subsequent decay. In light of this there is a need to better understand and quantify the impact of this exposure on the mechanical behaviour and capacity of such systems. Here an experimental investigation is presented which sets out a novel test method for measuring the impact of cyclic wind driven rain and flood exposure on the lateral stiffness and strength of masonry infilled timber frames. Empirical data presented here indicates losses in elastic stiffness exceeding 75% as a result of exposure, whilst analytical assessment confirms the failure mechanism that describes yielding of the system in weathered and unweathered states. This work has measured the extent of structural decay in direct relation to the meteorological parameters wind speed and precipitation accumulation, giving deeper, understanding of the vulnerability of the structural system of masonry infilled timber framing to these climate phenomena.

Introduction

Around the world precipitation levels are continuing to be observed to increase, linked to the rise in global mean temperature (IPCC, 2014), with ever more unprecedented accumulations leading to widespread flooding in the UK (Thompson, et al., 2017), and across Europe (Alfieri, Burek, Feyen, & Forzieri, 2015), the United States (Mallakpour & Villarini, 2015) and elsewhere across the globe (Hirabayashi, et al., 2013). Likewise there is evidence to suggest storm frequency has increased in the latter half of the 20th Century, especially in the Northern Hemisphere (Vose, et al., 2014), where observational evidence of increased storm activity in the North Atlantic since the 1970's exists (IPCC, 2007).

One consequence of this for the built environment is increased exposure of buildings to flood and storm conditions; that is strong winds, high rainfall accumulations and inundation by flood water. Historic masonry infilled timber frames (HMITF) are often highly prevalent in such affected urban centres, for example Prague (Holicky & Sykora, 2009) and York, (MacDonald, 2012). Flood and wind driven rain exposure lead to the saturation of absorbent historic façade fabric (Drdacky, 2010), such as the timber, mortar and infill material used in HMITF. Windstorms and floods expose facades to physical damage caused by loading from wind pressure (Holmes, 2015) and hydro-static or -dynamic loading (ASCE, 2006). The comparatively low strength and stiffness of HMITF leaves them potentially more susceptible to damage from wind and flood loading than modern framed buildings.

Investigation of climate change effects in relation to cultural heritage is a growing field of research application. Much work focusses on spatial risk assessments driven by

observational measures of building vulnerability, such as cultural significance either through formal scheduling (Wang, 2015) or community perception (Vojinovic, et al., 2016) and other factors such as age and condition (Stephenson & D'Ayala, 2014). Technical studies which garner evidence for the physical and mechanical vulnerability of heritage buildings are less common, and offer little insight into the structural impacts of climate change on historic structures.

Impact assessments focus on physical damage such as salt induced weathering (McCabe, et al., 2013), both stone (Sass & Viles, 2010) and brick masonry (Binda, Cardani, & Zanzi, 2010) wetting and drying regimes. Whilst vulnerability indicators and scales are emerging for cultural heritage at large spatial scales (Sabbioni, Brimblecombe, & Cassar, 2012), damage functions are typically limited to physical, chemical and biological damage (EU, 2015). These are derived from visual observations rather than investigation of cause and effect relationships, and do not acount for structural impacts of climate exposure.

Work seeking to understand and quantify the loss of structural integrity due to flooding does not typically examine historic building systems. Experimental work has focussed on the study of modern masonry blockwork in either solid (Herbert, Gardner, Harbottle, & Hughes, 2012) or cavity (Escarameia, Karanxha, & Tagg, 2007) wall form. Theoretical (Kelman & Spence, 2003) or probabilistic (Mebarki, Valencia, Salagnac, & Barroca, 2012) analyses of masonry vulnerability to flood depth are not directly relatable to historic construction systems; making use of modern material paramters, geometric forms and construction details. Comparable work which addresses the behaviour of historic timber framed structures to flooding is lacking from the knowledge

base, although studies investigating storm damage to traditional timber structures (Pazlar & Kramar, 2015) are beginning to emerge. More developed investigation of hazard-damage relationships for historic timber frames in earthquakes exists, including with masonry infills both with (Ferreira, Teixeira, Duta, Branco, & Goncalves, 2014) and without diagonal bracing (Duta, Sakata, Yamazaki, & Shindo, 2016).

National flood risk assessment (FRA) protocols typically compute losses on the basis of economic value. In the UK typologies relating to building purpose are used in FRA manuals (Penning Rowsell, Priest, Parker, & Tunstall, 2013), which do not account for the construction form of the exposed building stock associated with their historic nature. The equivalent US FRA model accounts for modern timber framing as a typology (FEMA, 2013), but gives no indication of its fit to historic timber frames. Damage scales embodying physical typology features often focus on building shape and form (Maiwald & Schwarz, 2012); (Kelman & Spence, 2004), with limited examples attempting to incorporate mechanical or structural parameters into the measure of vulnerability (Custer & Nishijima, 2015). With global damages from flood events leading to ever increasing costs (SwissRe, 2012), there is a pertinent need to examine the structural implications for historic structures so that future losses can be understood, predicted and appropriately managed.

The present work sets out a methodology for systematically investigating the structural response of historic masonry infilled timber frames (HMITF) to exposure to wind driven rain and flood. In the first section the experimental approach is described, which incorporates a novel methodology and test rig design for generating environmental weathering conditions for use in the laboratory as hazard scenarios. Reclaimed historic

building materials and traditional construction techniques are used to produce full-scale test specimens.Following environmental exposure structural testing is carried out to determine the mechanical response of the HMITF after weathering from flood and wind driven rain. The second half of the paper presents the empirical findings and the results of a theoretical assessment of the HMITF's under weathered conditions.

The case study location of Tewkesbury in Gloucestershire, a location prone to wind driven rain exposure, and which has suffered severe flooding (Figure 1) in recent decades (Marsh & Hannaford, 2007) was studied. The work forms part of the Parnassus project (www.ucl.ac.uk/parnassus), which took an interdisciplinary approach to the investigation of risks posed to the historic building stock from climate change. The project incorporated an on-site monitoring campaign to measure hygro-thermal effects of wind driven rain and flood on building fabric through the collection of concurrent climatic and materials response data (Aktas, D'Ayala, Erkal, & Stephenson, 2015). Work to determine the probabilistic flood risk at the site highlighted the significance of high resolution modelling in ascertaining building level exposure (Smith, Bates, Freer, & Wetterhall, 2014). Meanwhile a statistical study based on observations of building typologies led to the derivation of a vulnerability model for wind driven rain and flood exposure to historic structures (Stephenson & D'Ayala, 2014). The work presented here extends the outputs to the study of structural vulnerability of HMITF to flood and wind driven rain exposure.

Experimental Investigation

From Climate Hazard Data to Experimental Test Conditions

Review of fundamental knowledge and laboratory test protocols that focus on wind driven rain and flood exposure highlighted that whilst extensive understanding of these phenomena exist, experimental studies have tended to derive from simplistic recreation of the weathering conditions. Wind driven rain (WDR) exposure has been modelled and computed for many years, a review of which is provided by Blocken and Carmeliet (2010) and Stephenson (2016). Early work by Lacy (1971) led to the derivation of the empirical relationship shown below, which describes the relationship between wind speed (U), rainfall (R_h) and wind driven rain (R_{wdr}), the constant κ accounting for the maximum speed a raindrop will fall given terminal velocity effects.

$$R_{wdr} = \kappa\, U\, R_h \qquad (1)$$

Translation of this analytical formula into a measure of WDR exposure exists in the form of exposure maps published in BS 8104 (BSI, 1992), and more recently in BS EN ISO 15927-3 (BSI, 2009)(BSI, 2009) where a building oriented approach is taken. This computes exposure at the individual building scale using a spell based approach, although gives guidance only on the minimum threshold of rainfall accumulation and wind speed for WDR wetting to occur. D'Ayala and Aktas (2016) present a critical appraisal of the analytical and codified models referred to above, on the basis of the wind driven rain data collected at the site in Tewksbury within the Parnassus project. Current literature reporting on laboratory tests which measure wind driven rain impacts on historic building fabric, provides wetting rates that are not directly translateable back

to climatic conditions, rather provide guidance on total water volumes and test durations (Baker, Sanders, Galbraith, & Craig McLean, 2007a); (Sass & Viles, 2010).

The new method proposed herein takes reference from the location specific approach of exisiting British Standards, however looks to generate more specific weathering conditions which account for the extreme precipitation conditions which lead to flood events. This improves on the existing spell based approach by setting out exposure conditions using a finite temporal range. Meanwhile a cyclic approach provides realistic impacts of wind driven rain exposure over time, where wetting and drying cycles instigate fatigue in the construction system. This is especially appropriate for timber frame systems where cyclic exposure to moisture produce particularly damaging environmental conditions, due to the effects of moisture fluctuation on the breakdown of timber material and subsequent reduction in mechanical capacity (Stephenson, 2016).

The sequence design rationale identifies a total duration and volume of water for a given rainfall event, and disperses this using a rainfall intensity measure most likely to induce wetting in the construction materials. This reflects the fact that lower intensity rainfall allows for greater absorption of moisture into the fabric, as surface saturation effects are not significant (Hall & Kalimeris, 1982). It additionally links the rainfall to pluvial and groundwater flooding, which are those typically associated with more recurrent and prolonged floods. Whilst it is not possible to study the response of the materials and structural system at reduced temporal scale, the aim is to generate conditons suitable for studying long term effects.

The method of determining test flow rates is depicted in Figure 2 (where millimetres per square metre are equivalent to litres) and this was applied to the case study location of Tewkesbury using a 30-year daily precipitation data set covering 1981-2011, obtained from the Met Office's MIDAS system (MetOffice, 2012), from which an average daily precipitation total of 36 mm/day was calculated. This was then used in conjunction with 2m/s of wind speed, specified as the minimum wind speed generating "wetting conditions" in BS 15927-3 (BSI, 2009), and input into the WDR equation above to derive a total WDR amount of 10mm/day.

To encourage wetting of the wall the water was dispersed at the lowest possible intensity rate that correlated to the probability of occurrence of the rainfall amount. Studies by Holland (1960) highlighted the relationship between rainfall duration and intensity applicable to sites across the UK and this data set the threshold for use in this study (Figure 3). The duration of cycles was set so as to produce a feasible test procedure, which could be programmed to run automatically in a 24-hour period.

This ultimately determined a 3 hour wetting and drying cycle design of: 40 minutes of wetting, giving a flow rate of 0.375 L/minute, followed by a 2 hour and 20 minute period of drying of the wall. This individual cycle was then repeated a given number of times in order to produce a hazard scenario of given severity. Each of the wetting cycles corresponds to an approximately annually occurring wind driven rain event, such that 100 cycles represent 100 years of weathering. The flow rates used, being derived from observed data, do not account for any probabilistic climate change related increase in precipitation amounts. Rather these figures are intended to provide for a correlation of loss with weathering intensity based on measured precipitation rates.

Four HMITF's were tested in total, a control specimen tested with no wetting (Frame 1) and three further specimens tested under different conditions. Frame 2 was subject to a total of 100 cycles followed by a 100 year return period flood. Frame 3 was subject to this procedure twice, allowing for drying to original moisture content between each repetition. A final specimen, Frame 4, was used to test whether more dispersed cycling would pose greater risk to the structure. This was achieved by interrupting the weathering after every 10 cycles and drying the wall to original moisture content, continuing until 100 cycles had been applied and completing the test with the same 100 year return period flood. In each case the depth of flood was 0.75m for a period of 72 hours. These conditions were extracted from the flood model derived within the Parnassus project (Smith, Bates, Freer, & Wetterhall, 2014).

A bespoke test rig (Figure 4) was constructed to facilitate the weathering whilst also allowing for the full-scale specimens to be continuously loaded vertically in compression, to represent in-situ dead loading. The rig comprised the following principal components:

1. Hanging frame capable of supporting and measuring with electronic load cells the weight of the test specimens to a resolution of 500g continuously throughout the test procedure, to monitor the weight increase attributable to moisture ingress.
2. Steel plates situated immediately above and below the specimens linked with steel bars to be tensioned to apply a vertical compressive load of 10kN, calculated as representative of a two storey masonry infilled timber frame building typically to Tewkesbury.

3. Flood basin enclosing the specimen and providing capability of simultaneous internal and external flooding representative of a flood inundated building.
4. Spray nozzles capable of producing a range of water flow rates and incorporating an air supply such that the spray is atomised to best represent rainwater droplets.
5. Drying fans capable of producing an air flow of 2m/s across the surface of the test specimen, conditions requisite for drying in accordance with BS EN ISO 15927-3. As such no air pressure is simulated in the test procedure.

The water was applied to the face of the specimen using a spray nozzle from which a combination of air and water was dispersed, in order to create a droplet array representative of the wetting of the wall by rain droplets carried horizontally by wind. An actuator controlled the nozzle output, such that it could be programmed remotely and multiple cycles could be run continuously during the 24-hour period, without intervention by a technician.

In total 4 nozzles were used to provide coverage across the whole specimen, with each nozzle producing a spray cone of 60 degrees and situated 50 cm away from the face of the specimen. At maximum capacity each nozzle produces a flow of 1.8 L/minute, with the water atomised evenly across the area projected by the cone onto the surface. Floodwater was introduced to the basin independently by hand direct from the supply, ensuring the water used was free from debris that may have collected within the recirculation system, and also ensured a controlled rise of floodwater depth.

Drying of the wall was carried out using multiple fans generating a cross-flow of air on the surface of the specimens. This was monitored throughout the test using an

anemometer to ensure constant conditions. Air temperature was that of the ambient laboratory condition, which fluctuated between 18 and 22 degrees Celsius dependent upon time of day and season. Relative humidity within the laboratory fluctuated within a range of 55 to 65 %. These ambient conditions are recognised as being different from likely external conditions during a wind driven rain event, however manipulation of these were beyond the capacity of the laboratory facility.

Structural Test Procedure

On completion of the weathering test each frame specimen was subjected to a racking test carried out with reference to BS EN 594 (BSI, 2011), with fixing and loading conditions as in Figure 5. The test was carried out in a separate test rig, such that the specimen was no longer subject to any weathering once structural testing had commenced. This is typically used to measure loss of stiffness in timber frames and is therefore a globally recognised parameter of fatigue. The method is limited in its applicability to masonry infilled frames, in that it assumes larger deflections than would occur in a masonry infilled system (100mm), and this defines failure according to the test method. Additionally vertical point loading is specified, which does not account for the unifrom spead loads that a masonry infill will induce onto a timber frame.

In amendment of the standard therefore a vertical compression load of 10kN was applied uniformly across the top rail of the specimen using a hydraulic jack and spreader beam. Meanwile a cyclic in-plane lateral racking load was applied at the top right corner of the frame. In accordance with the standard, racking loads were stabilised for a time period of 300 +/- 60 seconds, alternated with unloaded periods of

the same duration. Increments of 1kN load were applied up to 10kN, at which point 2kN increments were used until failure was attained.

Displacement was measured using LVDT sensors, with the frame constrained by the spreader beam at the top, directly underneath which was sandwiched a strip of engineering cork to ensure good friction contact between the steel and the timber. The frame was fixed along its base to the steel base plate by portland cement mortar and was prevented from sliding using a steel restraint at its lower left corner. Timber baton restraints were also fixed to the loading frame, and used to restrict out of plane movement.

The lateral load was applied at the upper right corner of the frame (Figure 5, left), such that the end face of the top horizontal frame member received a point load and the frame was pushed into bending dependent upon the moment capacity of the mortise and tenon joints. Once any joints had mobilised, further loading resulted in sway developing within the timber frame, in addition to bending. Failure was assumed to have occurred when substantial cracking occurred in the masonry and increased loading was impossible. This coincided with a flattening of the backbone load displacement capacity curve for the frame, and so this condition also defined the ultimate load for the frame

The load and displacement data obtained from the test was used to determine the stiffness and strength of the composite timber frame and masonry infill system. The sway nature of the displacement of the frame subjects the infill to diagonal compression loading, and as such the shear stiffness of the masonry is contributory to

the stiffness exhibited by the whole system. To quantify this contribution, the effect of exposure to the weathering simulations on the masonry was independently assessed through the testing of masonry wallettes representative of the infill panel, as reported in Stephenson et al., (2016).

Test Specimens

The masonry infilled timber frame system replicated in the laboratory does not incorporate a bracing element (Figure 6). The type of construction used here is often seen in historic frames where a post and beam system is used to transfer loads across multiple bays in a single façade, and where bracing members are provided only at the corners. This particular design is especially vulnerable to racking effects from wind loading, such as would be present during a wind driven rain event due to the lack of bracing. Cyclic loading of the system will instigate sway and eventually permanent deflection as fatigue is instigated by the loading cycles. This therefore represents the worst case building typology with regards structural vulnerability of the system to this particular climatic condition.

The final design of the specimens was derived from structures observed on site in Tewkesbury (Figure 7). Joints between the cross-rails and uprights are constructed with a single oak peg mortice and tenon joint. The design of the frame reflects early English timber frame design, where large principal posts and beams were spaced at greater distances to provide doorways or window apertures (Brunskill, 2006). This also generates a more vulnerable structure, as the beam and post members will be under higher stress conditions due to increased spans and applied loads.

Each timber frame specimen was constructed using reclaimed oak originally used in construction approximately 200 years ago. Pieces were selected for use in the frames based upon their condition; being as much as possible free from knots, sapwood, twist and fungal or insect damage. Grading of the material in accordance with BS 5756, the code for visual hardwood grading (BSI, 2011) determined that the majority of the oak was grade TH1, the higher of the two possible grade outcomes.

The masonry infill was constructed from reclaimed bricks aged to around 1820 and selected due to their high absorption characteristics and their shallow dimension, allowing more courses in the test specimens. The bricks were laid with a non-hydraulic lime mortar in the ratio 1:2.25, as would typically be used at the time such frames were originally constructed (Davey, 1961). The masonry was laid in stretcher bond with a 10mm bed and cured inside the timber frames for a period of one year prior to testing, to allow for optimum strengthening of the mortar bonds. Render was not applied to the specimens to encourage wetting of the masonry and allow thorough investigation of the masonry damage after testing. This also reflects observations of buildings from site where render is missing.

Impact of Weathering on Racking Capacity

Empirical Data

Material Properties

Characteristic physical and mechanical properties of the timber and masonry infil were obtained from samples tested in accordance with the relevant British Standard (Table 1). The elastic modulus of the timber batons is comparable with a hardwood classification of D18, the lowest grade recognised by the UK Timber Classification

Board (TRADA, 2011). The masonry modulus of elasticity is lower than other published empirical historic masonry modulus values, however the weak non-hydraulic lime mortar is likely to have contributed significantly to this. Figures quoted in Table 1 also highlight that historic masonry properties can be highly variable across the world, with the age of the structure also a factor.

Table 1 Nominal and published values of strength and stiffness for timber and masonry

Moisture Uptake

Continuous weighing of the specimens during weathering demonstrated that the rate of uptake was initially very high, but reduced significantly after approximately the first 10 cycles, as exemplified in Figure 8 for Frame 2. The average total moisture content of the three frames ranged between 5% and 6% throughout the weathering test, largely accumulated in the initial uptake period. This is a relatively low moisture content, when compared to the 17% porosity of the bricks for example, highlighting the significance of even low level moisture accumulation on structural integrity.

Crack and Detachment Propagation Mapping

Visual assessment of the decay of the structure carried out on completion of the weathering test used tape measurement of masonry bond loss and infill panel-frame detachment, as shown in Table 2. The percentage of bond loss is a measure of the proportion of the total head and bed joint lengths within each infill panel section. The percentage of detachment is a measure of the proportion of the total possible length based upon the perimeter of the infill panel. In most cases these features were observed on both faces of the frame, especially in the case of bond loss between the frame and infill.

Table 2 Crack and detachment propagation under increasing weathering

Weathering caused considerable detachment to occur between the infill panel and frame for all three scenarios (Frames 2, 3, 4), with the final scenario causing 100% of the panel to detach in both the upper and lower portion. Bond loss also occurs in all scenarios and in both upper and lower panels, however the percentage is much lower than the percentage of detachment. Much greater vulnerability is identified therefore at the interface between the infill and frame, as oppose to in the masonry itself. The extent of detachment or bond loss is not proportional to the number of weathering cycles, possibly as a result of a number of parameters, such as the variation in the reclaimed materials used in the specimens, and the non-linearity in the response of those materials to increased water exposure when working as a composite system.

Racking Tests

The racking test load displacement cycles are presented in Figure 9, and the corresponding load-displacement envelopes are shown in Figure 10. Three phases of behaviour can be identified from the test data: (1) an initial phase of bedding in, with low values of stiffness increasing with displacement, most pronounced in Frames 3 and 4 where significant gapping was induced between the frame and infill as a result of the weathering; (2) a second phase where the stiffness of the composite system is exhibited; (3) a post-yield phase where the stiffness of the system reduces drammatically, following failure of one or more elements.

The elastic stiffness is defined from the first segment of each of the envelopes, and the yield point by the sudden shallowing of the load-displacement curve, indicated by

396 the crosses on the envelopes in Figure 10, at which point the yield strength is recorded
397 and remaining curve defines the yield stiffness. Table 3 sets out these key parameters
398 for the phases of behaviour of the frames. Both the elastic and yield stiffness's are
399 calculated in accordance with the below racking stiffness equation, given in BS EN 594
400 (BSI, 2011), and which calculates stiffness at the 10th (F_1) and 40th (F_4) percentile of
401 the maximum load, F_{max}. Here F_{max} is defined as the limit of proportionality in the initial
402 elastic region, and the maximum load applied to each frame in the case of yield
403 stiffness.

404 $$R = \frac{(F_4 - F_1)}{(d_4 - d_1)} \qquad (2)$$

405

406 *Table 3 Stiffness and strength characteristics of HMITF specimens*

407

408 Losses in elastic stiffness in the range 79-98% are measured across Frames 2, 3 and
409 4, demonstrating that weathering over the lifetime of a historic timber frame building
410 causes a substantial loss in structural integrity, even under pre-yield (service)
411 conditions. Less significant losses in yield strength were observed, up to 36% in Frame
412 4, with Frame 3 recording a yield strength comparable to the unweathered Frame 1.
413 This could be attributed to the weathering impact largely affecting the interfaces
414 between components in the HMITF's, such as masonry bonds, which contribute to
415 overall loss of stiffness, and having less significant impact on the overall strength of
416 the system.

417

418 The bedding-in phase which develops at the beginning of structural loading and only
419 after considerable weathering, demonstrates that the potential for damage induced by
420 rocking and sway in these frames in-situ is considerable, and directly attributable to

421 weathering from the environment as oppose to structural fatigue induced by any
422 loading time-history. Further loss of stiffness post-yield is accounted for by the higher
423 loading of the frame during the post-yield phase, and the observation that the joints
424 are being loaded beyond their yield point into permanently deformed states.
425
426 Structural cracking was measured throughout the duration of the loading cycles for
427 each frame, with the final observed patterns shown in Figure 11 for Frame 1, whilst
428 Figures 12, 13 and 14 show structural cracking compared to weathering induced
429 cracks for Frames 2, 3, and 4 respectively. The shape of the structural crack pattern
430 observed after the racking tests was similar for all the frames; staggered cracks
431 developed within the mortar joints and travelled diagonally from bottom left to top right
432 of the panels. This is in accordance with a compression load applied at the top left and
433 bottom right (Figure 16), which ultimately leads to tension cracks along the instigated
434 diagonal axis of the panel. For each of the progressively more weathered specimens,
435 cracking extended through the masonry at a lower load level.
436
437 Structural cracking was observed in Frame 1 in the load range 18-20kN. This reduced
438 to the range 15-18kN for Frame 2, 8-16kN for Frame 3 and 2-6kN for Frame 4. This
439 indicates a progressive reduction in shear capacity in the masonry, as was also
440 observed in the independent testing of masonry panels exposed to the same
441 weathering regime (Stephenson, Aktas and D'Ayala, 2016). Cracking in Frame 4 as a
442 result of the weathering was so extensive that independent structural cracks did not
443 develop in the masonry as a result of lateral loading. Rather some of the weathering
444 cracks acted as mechanisms for displacement, such as for example the large crack in

the top left corner of the lower panel, which opened up on loading of the frame (as shown by the yellow arrows in Figure 14).

Observations made during the testing of Frames 1 and 2 suggest that loss of elastic behavior was as a direct result of bond failure of both head joints and bed joints in the masonry, and that the stiffness exhibited after this point was contributed mainly by the timber elements, and the frictional rotation of the mortise and tenon joints. The joints were observed to rotate and localised crushing of fibres around the tenon was recorded, however rupture of the oak peg holding the joint together did not occur in any of the load tests, only minor permanent bending was observed on their removal after the test (Figure 15). In the following section the empirical evidence for vulnerability is expanded on with an assessment of the timber frames load-deflection behavior.

Assessment of Infilled Timber Frame Behaviour

Analysis of masonry infilled concrete or steel frames often applies the diagonal strut approach (Crisafulli & Carr, 2007), (Nassirpour & D'Ayala, 2017). The assessment developed and presented by the authors here also incorporates this approach, within the following method. The frame is first considered in elastic bending, and the masonry infill is assessed as a shear panel. Shear deformation can cause either horizontal sliding of masonry courses (pure shear), or a combined tension failure in the head joints with shear failure in the bed joints, which instigates the diagonal crack in the masonry. As the system reaches yield condition and deflection increases, failure is either as a consequence of joint rupture as rotation increases, or by diagonal compression in the masonry panel.

469 At this stage the frame is considered to act as a pin-jointed system, such that the
470 masonry infill acts as a diagonal strut within the frame, loaded in compression. The
471 progression of this failure mechanism is described in Figure 16. In the case of the
472 specimens here the presence of multiple diagonal cracks off the main axis of the panel
473 supports the use of the diagonal strut model for assessing post crack behaviour.
474 Timber connection rupture was not observed in the specimens, and the constant
475 stiffness observed on re-loading of the frame after multiple cycles suggests
476 deformation was as a result of reduced stiffness in the masonry infill alone.
477
478 Holmes (1961) was the first to suggest a method for approximating strut width from
479 panel dimensions. Later work by Stafford-Smith (1966) introduced the use of a
480 dimensionless parameter (λ_h), representing the relative stiffness of frame and infill, to
481 calculate the strut width. Mainstone (1971) set out the method for determining strut
482 geometry used here, theorising that following the formation of cracks in the panel two
483 or more struts are assumed to develop in the region bounding the cracks with the width
484 of the effective strut calculated in accordance with Equation 3 below, where d_{inf} and
485 H_{inf} represent the diagonal length and height of the infill panel respectively.
486
487 $$w = 0.16\, d_{inf}\left(\lambda_h H_{inf}\right)^{-0.3} \qquad (3)$$
488
489 Applying this principle, the struts identified in the specimens in this experimental
490 programme are shown in Figure 17. These are used to calculate the dimensions of an
491 effective masonry strut, and in conjunction with reduced masonry modulus are used to
492 calculate the expected deformation in the frame in the post-yield phase. Full detail of
493 this assessment is provided in Appendix A.

Elastic and Pre-Yield Behaviour in Unweathered Frame 1

In the unweathered case the frame is first assessed under pre-yield conditions at 10kN lateral load, so that the stiffness of the system when structurally robust is quantified and the application of the diagonal strut method at yielding is placed within this context. The timber frame is assumed to act as a portal frame with moment transferring joints, and the slope deflection method applied. Meanwhile the masonry panel is considered in combined shear and bending to determine lateral deflection. These two values define the upper and lower bound of expected deflection in the composite system. Full assessment is given in Appendix A, which yields a frame deflection of 4 mm, and shear deflection in the masonry of 0.86 mm. Frame 1 (unweathered) displayed a deflection of 0.8 mm at 10 kN of lateral load, showing the masonry infill dominates behaviour in the elastic range.

Yielding of Frame 1 occurred at 14 kN, at which point the diagonal strut model is assumed to be applicable, with the effective strut width taken as the diagonal length of the panel, according to Mainstone (1971). Applying the principle of virtual work to a pin-jointed truss braced with the masonry strut, the predicted overall deflection is calculated as 1.2 mm (Appendix A), whilst the observed deflection in Frame 1 at yield load was 2mm. Assuming the masonry panel is still acting in combined shear and bending, the masonry deflection is calculated as 1.7mm at 14kN of load. The observed behavior in the unweathered frame suggests that at yielding the masonry stiffness is again dominating behavior of the overall system.

It is also true that a full pin joint likely did not develop in the frame at 14kN, as the geometry of the mortise and tenon joint and the presence of the dowel, generating frictional restraint, prevents free rotation, thus limiting the extent of lateral deflection compared with the theoretical hinge. Detailed assessment of the rigidity of the mortise and tenon joint is beyond the scope of this work, however is clearly an important issue for consideration in future studies (Quinn, D'Ayala, & Descamps, 2016).

Post-Crack Behaviour in Frames 1, 2, 3 and 4

Applying the struts as shown in Figure 17 the theoretical deflection in Frames 1 to 4 is calculated at the lateral load corresponding to maximum cracking, highlighted in the envelopes in Figure 10. The table below compares the deflection observed in the post-yield portion of the envelope up to final cracking load, with the theoretical deflection according to the diagonal struts extracted from the crack patterns, computing also the percentage difference between empirical and analytical values.

Table 4 Comparison of observed and theoretical deflection

The theoretical model computes a deflection that is less than the observed in all cases, by between 2 and 17%. The difference values are comparable with Stafford-Smith's difference of 15%, observed between experimental test and theoretical work when the non-dimensional parameter λ was first proposed (1962). The increase in difference values may be attributable to the variance in timber elastic modulus, which would be larger than in concrete. Additionally, the elastic modulus of the masonry panels may not correspond to the value of E obtained from separate wallet testing carried out for material characterization (Stephenson, Aktas & D'Ayala, 2016)

The comparable results between empirical and theoretical work, demonstrates that the mode of failure in the weathered system is that of the compression strut. The tests and associated calculations demonstrate that the weathering leads to a measureable reduction in racking stiffness as a consequence of loss of bond in the masonry due to this weathering leading to reduced compression strut area. This sets out a quantifiable link between exposure to wind driven rain and flood, and loss of structural integrity in this type of historic construction system.

Vulnerability to Wind Loading

The findings above have further consequences for the resistance of the system to wind loading. The cyclic lateral loading of the timber frames is comparable to the conditions a timber frame building would be subject to during a windstorm. The behaviour of the infilled timber frame is therefore placed in the context of the hazard by converting the loads sustained by the frames into comparable wind loading conditions. Typical UK average (Met Office, 2016) and 0.02 exceedance (50 year return period) wind speeds (BSI, 2005) are shown in Table 5, along with values specific to the case study location of Tewkesbury.

Table 5 Wind speeds for UK and Tewkesbury average and 50 year return periods

In Table 6 the loads applied at the yielding of the timber frames are converted into wind speeds, and compared with the load that corresponds with the 20 m/s wind speed applicable to a 1 in 50 year event in Tewkesbury. The loads are converted back to wind speeds by applying the procedure set out in BS EN 1994-1-4 in reverse, to determine first wind pressure and then wind speed. Terrain, turbulence and other relevant factors

569 are all assumed to be 1, meanwhile the area on which the wind pressure is assumed
570 to act corresponds to the 1.5 m^2 area of the test panels.
571
572 The yield loads are higher than the average or storm conditions identified by codified
573 data or national databases. However, they are of comparable size to typical UK gust
574 winds even in low-level zones. For example, the record gust speed for the region in
575 which Tewkesbury is located (Midlands) is 114 mph (50 m/s) for sites below 500m
576 AMSL (Met Office, 2016).
577
578 *Table 6 Conversion of empirical loadings conditions into generic wind speeds*
579
580 When considering the 0.02 exceedance value as an equivalent lateral load of 3.75 kN,
581 the increase in displacement displayed by the frames as they are exposed to more
582 severe weathering in notable. In the unweathered sample this load led to a
583 displacement of 0.15 mm, whilst after 100 cycles 1.4 mm of displacement was
584 recorded, and after 200 cycles, 3.25 mm. In the case of Frame 4 where the wetting
585 and drying was extended with longer drying periods, this displacement had increased
586 to 9mm.
587
588 This trend is shown in Figure 18 where the displacement is correlated with the total
589 test duration in hours, which was used in order to derive a single measure of hazard
590 severity that could be applied to the different weathering simulations. A second order
591 polynomial relationship is fitted to the data, and highlights that there is an increasing
592 rate of loss observed as the hazard increases, described by the upwards curve of the
593 trend line. Upwards trends in hazard severity as climate change further unfolds

indicates that in the future these construction systems are likely to demonstrate ever more increasing levels of loss and damage.

The extent of deflection in Frame 4, coupled with the increased rate of loss over time presents this structural system as highly vulnerable to exposure of this kind. A deflection of 9mm could lead to considerable damage to internal finishes, or instigate further structural damage such as at connections to roof elements. This finding highlights the importance of quantifying these relationships, so that the level of risk associated with the interaction of the structure and the hazards can be identified and its significance presented to both the conservation and engineering communities.

Conclusions

- Structural tests have demonstrated that a cause and effect relationship exists between exposure to wind driven rain and flood and loss of structural integrity in historic masonry infilled timber frames.
- Racking stiffness assessment demonstrates that the weathering alters and reduces the construction system integrity such that the failure mechanism of the system changes from a shear failure to a diagonal compression failure.
- Good correlation is found between weathering crack patterns and loss of stiffness due to diagonal strut geometry change, highlighting that weathering assessment can be used to predict loss of structural integrity in masonry infilled timber frames.
- Assessment under wind loading demonstrates that even under moderate wind conditons loss of stiffness due to weathering leads to substantial deflections in the system, such as would cause secondary damage to buildings and finishes.

- An increasing rate of integrity loss as weathering severity increases is deomnstrated for this construction system, highlighting significant vulnerability of this historic building typology to this climate hazard.

This programme of testing represents one of the first attempts to generate empirical measures of the fragility of traditional brick masonry infilled timber framed structural systems to exposure to flood and wind driven rain hazards. The derivation and execution of the test procedure is in itself novel, meanwhile the test results have highlighted that a significant amount of risk is posed to these structures by such hazards. The findings are not yet conclusive in every regard and are only applicable to the specific materials, masonry and frame system used. However, the data has provided initial quantification of the extent of material and structural degradation caused to this specific structural system by cyclic exposure to wetting and drying, and simulated flood conditions. Furthermore a clear relationship between the loss of yield stiffness and exposure duration has been derived, both from empirical and theoretical methods, which sets out an envelope of fragility in which the system can now be considered.

The findings of the investigation highlight that the structural risks are both real and measureable, although they are derived from a deterministic methodology. It is hoped that this technical information will aid the heritage community in prioritising and managing further mitigation activities, now that the scope and nature of the problem is described quantitatively and in more detail. In addition to assessment of other structural systems, a key next step for the work is the derivation of a probabilistic methodology which achieves the same physical assessment goals. This will ensure

643 that the findings of the structural and weathering analysis procedures are incorporated
644 into future risk assessment protocols surrounding the impacts of wind and precipitation
645 on historic timber frame structures, the pursuance of which will promote and progress
646 risk reduction goals for the heritage community.
647
648 **Appendix A**
649
650 **Elastic Phase – Slope Deflection Assessment**
651 First the elastic case is considered using the slope deflection method (Figure 19),
652 applying the general equation:

653 $$M_{ij} = \frac{2EI}{L}\left(2\theta_i + \theta_j\right) + \frac{WL^2}{12}$$

654 (4)

655
656 Applying horizontal and vertical equilibrium gives:

657 $$M_{AC} + M_{AB} = 0$$

658 $$M_{BA} + M_{BD} = 0$$

659 $$M_{CA} + M_{CE} + M_{CD} = 0$$

660 $$M_{DB} + M_{DC} + M_{DF} = 0p$$

661 $$M_{AC} + M_{CA} + M_{BD} + M_{DB} = 7.5$$

662 $$M_{CE} + M_{EC} + M_{DF} + M_{FD} = 7.5$$

663 (5)

664 Substituting (4) into (5) and applying Gaussian Elimination produces the following set
665 of equations written in matrix format:

$$\mathbf{EI}\begin{bmatrix} \frac{28}{3} & 2 & \frac{8}{3} & 0 & \frac{96}{9} & 0 \\ 2 & \frac{28}{3} & 0 & \frac{8}{3} & \frac{96}{9} & 0 \\ \frac{8}{3} & 0 & \frac{44}{3} & 2 & \frac{96}{9} & \frac{96}{9} \\ 0 & \frac{8}{3} & 2 & \frac{44}{3} & \frac{96}{9} & \frac{96}{9} \\ 8 & 8 & 8 & 8 & \frac{384}{9} & 0 \\ 0 & 0 & 8 & 8 & 0 & \frac{384}{9} \end{bmatrix}\begin{bmatrix} \theta_A \\ \theta_B \\ \theta_C \\ \theta_D \\ \delta_1 \\ \delta_2 \end{bmatrix} = \begin{bmatrix} \frac{-10}{12} \\ \frac{-10}{12} \\ 0 \\ 0 \\ 7.5 \\ 7.5 \end{bmatrix} \quad (6)$$

Using values of *E* from the timber baton tests (Table 1), *I* is calculated from a member cross section of 120 x 120 mm, giving I = 17.28 x 10^6 mm. Solving for values of θ and δ gives:

$\theta_A = -0.00356\, rad$ $\theta_B = -0.00356\, rad$

$\theta_C = -0.00389\, rad$ $\theta_D = -0.00389\, rad$

$\delta_1 = 4.2\, mm$ $\delta_2 = 2.8\, mm$

Rotational values of θ are converted to lateral movement through multiplication by the height of the sway mechanism, which is 750 mm in the case of these frames. This gives a total deflection in the frame of 4 mm.

Calculating the deflection of the masonry infill in combined shear and bending, using the formula given by Hendry et al. (1997) for a panel constrained only at the base:

$$\delta = \frac{Wh^3}{3EI} + \frac{\lambda Wh}{A\,G} \quad (7)$$

where the height (*h*), shear area (*A*) and second moment of area (*I*) are calculated from the panel dimensions of 575 x 820 x 120 mm. The shear modulus (*G*) equals 40%

686 of *E* (BSI, 2012), giving G = 164 N/mm^2 and λ = 1.2. This gives the predicted shear
687 deflection of the masonry as 0.86 mm, indicating that the masonry stiffness dominates
688 the overall racking stiffness in the pre-yield state.
689
690 **Post Crack Phase - Diagonal Strut Assessment**
691 The diagonal strut model (Figure 20) is applied and the pin-jointed truss assessed
692 using virtual work, for five cases: Frame 1 at pre-yield and post-crack, and Frames 2,
693 3 and 4 at post-crack.
694
695 Deflections are computed below for estimated strut geometries as shown in Figure 17.
696 The initial masonry stiffness is calculated from compression testing of the masonry
697 units and mortar, according to Eurocode 6 (BSI, 2012). This gives a compressive
698 strength for the masonry of 4.1 MPa, an acceptable value for historic masonry.
699
700 Converting to the elastic modulus requires the application of a constant, K_E. Reporting
701 on appropriate values of K_E range from 1000 (EC6), through to observed values as low
702 as 250 (Narayanan & Sirajuddin, 2013). The observed value of stiffness calculated
703 from tests by these authors for masonry panels tested in isolation was 163 MPa,
704 corresponding to a K_E value of 40. For analysis however, a more conservative K_E value
705 of 100 is used. For each weathered frame an estimated reduced value of *E* is used,
706 reflecting the loss of stiffness exhibited by the masonry when tested separately in
707 combined compression and lateral loading (Stephenson, Aktas & D'Ayala, 2016). The
708 masonry modulus values used are:
709
710 Frame 1: E = 410 N/mm^2 Frame 2: E = 382 N/mm2,

Frame 3: E = 382 N/mm2 Frame 4: E = 210 N/mm2

The strut width is defined by Stafford-Smith and Carter (1969) and Mainstone (1971) using the following equations, where λ_h is a dimensionless parameter accounting for the relative stiffness of the infill panel and frame, and w is the width of the strut:

$$\lambda_h = \sqrt[4]{\frac{E_{inf} t \sin 2\theta}{4 E_c I_c H_{inf}}} \quad (8)$$

$$w = 0.16\, d_{inf} \left(\lambda_h H_{inf}\right)^{-0.3} \quad (9)$$

where:

E_{inf} = Panel Elastic Modulus t = Panel Thickness

H_{inf} = Panel Height ɵ = Angle Panel Diagonal to Horizontal

E_c = Frame Elastic Modulus I_c = Frame Moment of Inertia

d_{inf} = Diagonal Length of Strut

For each identified strut (shown in Figure 17) the diagonal length is measured (d_{inf}) and the associated strut width calculated from Equation 9.

Table 7 Deflection of Frame 1 at yield load (14kN)

Table 8 Deflection of Frame 1 at post-cracking (21kN)

Table 9 Deflection of Frame 2 at post-cracking (18kN)

Table 10 Deflection of Frame 3 at post-cracking (16kN)

Table 11 Deflection of Frame 4 at post-cracking (6kN)

Acknowledgments

The authors would like to thank those who assisted with the experimental portion of this work, the laboratory technicians in the Department of Civil, Environmental and Geomatic Engineering at UCL. This work was funded by the Science and Heritage Programme in the UK, under the project Parnassus (AH/H032525/2).

References

Aktas, Y., D'Ayala, D., Erkal, A., & Stephenson, V. (2015). Environmental performance assessment using monitoring and DVS testing. Proceedings of the ICE - Engineering History and Heritage, 168(1), 3-16.

Alfieri, L., Burek, P., Feyen, L., & Forzieri, G. (2015). Global warming increases the frequency of river floods in Europe. *Hydrol. Earth Syst. Sci., 19*, 2247-2260.

Aras, F., & Altay, G. (2015). Investigation of mechanical properties of masonry in historic buildings. *Gradevinar*, 67 (5) 461-469.

ASCE. (2006). *ASCE/SEI 7-05 Minimum design loads for buildings and other structures.* ASCE.

Baker, P., Sanders, C., Galbraith, G., & Craig McLean, R. (2007a). Blickling Hall basement case study. In M. Cassar, & C. Hawkings, *Engineering Historic Futures* (pp. 19-39). London: University College London.

Barredo, J. (2009). Normalised flood losses in Europe: 1970-2006. *Natural Hazards and Earth System Sciences, 9*, 97-104.

Binda, L., Cardani, G., & Zanzi, L. (2010). Non-desctructive Testing Evaluation of Drying Processes in Flooded Historic Masonry Walls. *ASCE J. of Perform. Const. Facil, 24*(5).

Blocken, B., & Carmeliet, J. (2010). A review of three state of the art wind driven rain assessment models and comparison based on model theory. *Building and Environment, 45*(3), 691-703.

Brunskill, R. (2006). *Timber Building in Britain.* Yale University Press.

BS. (1957). *BS 373 Structural Testing of Small Clear Specimens.* London: BSI.

BSI. (1992). *BS 8104 Code of practice for assessing exposure of walls to wind driven rain.* London: British Standard.

BSI. (2005). *Eurocode 1: Actions on Structures. Part 1-4: Genral actions - wind actions.* London: BSI.

BSI. (2009). *BS EN 15927-3:2009 Hygrothermal performance of buildings. Calculation and presentation of climatic data. Calculation of a driving rain index for vertical surfaces from hourly wind and rain data.* London: BSI.

BSI. (2011). *BS 5756:2007+A1:2011 Visual Grading of Hardwoods.* London: BSI.

BSI. (2011). *BS EN 594 Timber Structures. Timber Methods. Racking strength and stiffness of timber frame wall panels.* London: British Standards.

BSI. (2012). *Eurocode 6: Design of Masonry Structures.* BSI.

Crisafulli, F., & Carr, A. (2007). Proposed Macro-Model for the Analysis of Infilled Frame Structures. *Bulletin of the New Zealand Society for Earthquake Engineering*, 40 (2) 69-77.

Crisafulli, F., Carr, A., & Park, R. (2000). Analytical Modelling of Infilled Frame Structures - A General Review. *Bulletin of the New Zealand Society for Earthquake Engineering*, 33 (1) 30-47.

Custer, R., & Nishijima, K. (2015). Flood vulnerability assessment of residential buildings by explicit damage process modelling. *Natural Hazards*, 461-496.

Davey, N. (1961). *A history of building materials.* London.

D'Ayala, D., & Aktas, Y. (2016). Moisture dynamics in the masonry fabric of historic buildings subjected to wind-driven rain and flooding. *Building and Environment 104*, 208-220.

Drdacky, M. (2010). Flood Damage to Historic Buildings and Structures. *J. Perform. Constr. Facil.*, *24*(5).

Drdacky, M., Binda, L., Hennen, I., Kopp, C., Lanza, L., & Helmerich, R. (2011). *CHEF - Cultural Heritage Protection Against Flooding.* Prague: Institute of Theoretical and Applied Mechanics.

Duta, A., Sakata, H., Yamazaki, Y., & Shindo, T. (2016). In-Plane Behaviour of Timber Frames with Masonry Infills under Static Cyclic Loading. *ASCE Journal of Structural Engineering, 142*(2).

Escarameia, M., Karanxha, A., & Tagg, A. (2007). Quantifying the flood resilience proerties of walls in typical UK dwellings. *Building Services Engineering Research and Technology, 28*(3), 249-263.

EU. (2015). *Built Cultural Heritage in Times of Climate Change* (1st ed.). (J. Leissner, U. Kaiser, & R. Kilian, Eds.) Leipzig: Fraunhofer MOEZ.

FEMA. (2013). *HAZUS-MH Flood Technical Manual.* Washington: FEMA.

Ferreira, J., Teixeira, M., Duta, A., Branco, F., & Goncalves, A. (2014). Experimental Evaluation and Numerical Modelling of Timber-Framed Walls. *Experimental Techniques, 38*, 45-53.

Hall, C., & Kalimeris, A. (1982). Water movement in porous media V: Absorption and shedding of rain by building surfaces. *Building and Environment, 17*(4), 257-262.

Hendry, A., Sinha, B., & Davies, S. (1997). *Design of Masonry Structures* (3rd Edition ed.). London: E & FN Spon.

Herbert, D., Gardner, D., Harbottle, M., & Hughes, T. (2012). The strength of masonry walls when subject to flood loading. *15th Brick and Block Masonry Conference* . Florianopolis. Brazil.

Hirabayashi, Y., Mahendran, R., Koirala, S., Konoshima, L., Yamazaki, D., Watanabe, S., . . . Kanae, S. (2013). Global flood risk under climate change. *Nature Climate Change (Letters), 3*, 816-821.

Holicky, M., & Sykora, M. (2009, October). Assessment of Flooding Risk to Cultural Heritage in Historic Sites. *Journal of Performance of Constructed Facilities, 24*(5).

Holland, D. (1960). The intensity of rainfall in the British Isles. In M. Office, *British Rainfall.* London: HMSO.

Holland, D. (1960). The intensity of rainfall in the British Isles. *British Rainfall (Met Office).*

Holmes, J. (2015). *WInd loading of structures.* (3. Edition, Ed.) Taylor and Francis.

IPCC. (2007). *Climate Change 2007: Synthesis Report. Contribution of Working Groups I, II and III to the Fourth Assessment Report of the Intergovernmental Panel on Climate Change.* Geneva: IPCC.

IPCC. (2014). *Climate Change 2014: The Synthesis Report.* Cambridge: Cambridge University Press.

Kelman, I., & Spence, R. (2003). A limit analysis of un-reinforced masonry failing under flood water pressures. *Masonry International, 16*(2), 51-61.

Kelman, I., & Spence, R. (2004). An overview of flood actions on buildings. *Engineering Geology, 73*(3-4), 297-309.

Kouris, L., & Kappos, A. (2012). Detailed and simplified non-linear models for timber-framed masonry structures. *Journal of Cultural Heritage*.

Lacy, R. (1971). *BRE Digest 127: An index of exposure to driving rain.* London: Building Research Establishment.

MacDonald, N. (2012). Trends in flood seasonality of the River Ouse (Northern England) from archive and instrumental sources since AD1600. *Climatic Change, 110*(3), 901-923.

Maiwald, H., & Schwarz, J. (2012). Damage and loss prediction model considering inundation level, flow velocity and vulnerability of building types. *WIT Transactions on Ecology and the Environment, 159.*

Mallakpour, I., & Villarini, G. (2015, March). The changing nature of flooding across the central United States. *Nature Climate Change (Letters), 5*, 250-254.

Marsh, T., & Hannaford, J. (2007). *The summer 2007 floods in England and Wales: a hydrological appraisal.* Centre for Ecology and Hydrology.

McCabe, S., Smith, B., McAlister, J., Gomez-Heras, M., McAllister, D., Warke, P., . . . Basheer, P. (2013). Changing climate, changing process: implications for salt transportation and weathering within building sandstones in the UK. *Environmental Earth Sciences, 69*(4), 1225-1235.

Mebarki, A., Valencia, N., Salagnac, J., & Barroca, B. (2012). Flood hazards and masonry constructions: a probabilistic framework for damage, risk and resilience at urban scale. *Nat. Hazards Earth Syst. Sci., 12*, 1799-1809.

MetOffice. (2012). Met Office Integrated Data Archive System (MIDAS) Land and Marine Surface Stations Data (1853-current). NCAS British Atmospheric Data Centre.

Narayanan, S., & Sirajuddin, M. (2013). Properties of Brick Masonry for FE Modelling. *American Journal of Engineering Research*, 1 6-11.

Nassirpour, A., & D'Ayala, D. (2017). Seismic loss estimation of mid-rise masonry infilled steel frame structures through incremental dynamic analysis. *Int. J. Forensic Eng.*, 3(3) 255-275.

Parajuli, H. (2012). Determination of mechanical properties of the Khatmandu World Heritage brick masonry buildings. *15th World Conference on Earthquake Engineering.* Lisbon, Portugal.

Pazlar, T., & Kramar, M. (2015). Traditional Timber Structures in Extreme Weather Conditions. *International Journal of Architectural Heritage, 9*(6), 689-695.

Penning Rowsell, E., Priest, S., Parker, D., & Tunstall, S. (2013). *Flood and Coastal Erosion Risk Management: A Manual for Economic Appraisal.* London.

Poletti, E., Vasconcelos, G., & Laurenco, P. (2015). Timber Frames as an Earthquake Resisting System in Portugal. In M. Correia, P. Laurenco, & H. Varum, *Seismic Retrofitting: Learning from Vernacular Architecture* (p. 161). CRC Press, Taylor and Francis.

Quinn, N., D'Ayala, D., & Descamps, T. (2016). Structural Characterisation and Numerical Modelling of Historic Quincha Walls. *Int. J. Arch. Heritage*, 10 (2-3) 300-331.

Sabbioni, C., Brimblecombe, P., & Cassar, M. (2012). *The Atlas of Climate Change Impact on European Cultural Heritage.* Luxembourg: Anthem Press.

Sass, O., & Viles, H. (2010). Wetting and drying of masonry walls: 2D resistivity monitoring of driving rain experiments on historic stone in Oxford, UK. *Journal of Applied Geophysics, 70*, 72-83.

Smith, A., Bates, P., Freer, J., & Wetterhall, F. (2014). Investigating the application of climate models in flood projection accross the UK. *Hydrological Processes, 28*(5), 2810-2823.

Stafford-Smith, B. (1966, Feb.). Behaviour of square infilled frames. *Proceedings Am. Soc. Civ. Engrs., 92*, 381-403.

Stafford-Smith, B., & Carter, C. (1969, Sep.). A method of analysis for infilled frames. *Proceedings of the ICE, 44*(1), 31-48.

Stephenson, V. (2016). *Vulnerability of historic structures to environmental actions; an empirical methodology. PhD Thesis.* University College London.

Stephenson, V., & D'Ayala, D. (2014). A new approach for flood vulnerability assessment for historic buildings in England. *Nat Hazards and Earth Syst Sci, 14*, 1035-1048.

Stephenson, V., Aktas, Y., & D'Ayala, D. (2016). Assessment of flood and wind driven rain impact on mechanical properties of historic brick masonry. *RILEM Materials, Systems and Structures in Civil Engineeing Conference.* Lyngby, Denmark, August 22nd to 25th.

SwissRe. (2012). *Flooding: an underestimated risk. Inspect, inform, insure.* Zurich: Swiss Re.

Thieken, A., Muller, M., Kreibich, H., & Merz, B. (2005). Flood damage and influencing factors: insights from the 2002 floods in Germany. *Water Resources Research, 41*.

Thompson, V., Dunstone, N., Scaife, A., Smith, D., Slingo, J., Brown, S., & Belcher, S. (2017). High risk of unprecedented UK rainfall in the current climate. *Nature Communications 8 (107).*

TRADA. (2011). *Wood Information Sheet 4: Timber strength grading and strength classes.* London: TRADA.

Vojinovic, Z., Hammon, M., Golub, D., Hirunsalee, S., Weesakul, S., Meesuk, V., . . . Abbott, M. (2016). Holistic approach to flood risk assessment in areas with cultural heritage: a practical application in Ayutthaya, Thailand. *Natural Hazards, 81*(1), 589-616.

Vose, R., A. S., Bourassa, M., Pryor, S., Barthelmie, R., Blanton, B., . . . Young, R. (2014, March). Monitoring and Understanding Changes in Extremes: Extratropical Storms, Winds and Waves. *Bulletin of the American Meterological Society*, 377-386.

Wang, J. (2015). Flood risk maps to cultural heritage: measures and process. *Journal of Cultural Heritage, 16*(2), 210-220.

916 *Table 1 Nominal and published values of strength and stiffness for timber and masonry*

Property	Value (MPa)	Standard/Reference
Timber Flexural Strength	64	BS 373
Timber Elastic Modulus in Bending	7486	BS 373
Masonry Shear Strength	0.105	EC 6
Masonry Elastic Modulus	163	BS EN 594
Masonry Shear Modulus	65	EC 6
Elastic Modulus_Istanbul (19^{th} C)	2500	Aras & Altay (2015)
Elastic Modulus_Khatmandu (18^{th} C)	274	Parajuli (2012)

917

918

Table 2 Crack and detachment propagation under increasing weathering

Frame Number	**Infill Detachment**		**Masonry Bond Loss**	
	Damage (%)		Damage (%)	
	Upper Panel	Lower Panel	Upper Panel	Lower Panel
Frame 1	0	0	0	0
Frame 2	75	69	10	3
Frame 3	49	60	7	6
Frame 4	100	100	2	7

927 *Table 3 Stiffness and strength characteristics of HMITF specimens*

928

Frame Number	Elastic Stiffness (N/mm)	Loss of Elastic Stiffness (%)	Yield Strength (kN)	Loss of Yield Strength (%)	Yield Stiffness (N/mm)	Loss of Yield Stiffness (%)
1	12000	-	14.0	-	330	-
2	2536	79	12.0	14	440	-
3	1071	91	14.0	-	280	15
4	200	98	9.0	36	0	100

929

930

931 *Table 4 Comparison of observed and theoretical deflection*

Frame No.	Final Crack Load (kN)	Observed Deflection (mm)	Theoretical Deflection (mm)	Percentage Difference (%)
1	20	16	13.3	-17
2	18	11.5	11.3	-1.7
3	16	12	10.0	-17
4	6	8	7.7	-3.8

932

933

934 *Table 5 Wind speeds for UK and Tewkesbury average and 50 year return periods*

Wind Condition	Wind Speed (m/s)
UK_Mean	6.5
UK_0.02	25.5
Tewkesbury_Mean	3.5
Tewkesbury_0.02	20

935

936

937 *Table 6 Conversion of empirical loadings conditions into generic wind speeds*

Frame Number	Load (kN)	Wind Pressure (kN/m2)	Wind Speed (m/s)
1	15	10	40
2	12.5	8.3	36.5
3	14	9.3	38.6
4	9	6	31.0
Tewkesbury 0.02	3.75	2.5	20.0

938

939

940

941 *Table 7 Deflection of Frame 1 at yield load (14kN)*

Member	E (N/mm2)	Length (mm)	Area (mm2)	Force (kN)	Deflection, δ (mm)	Unit Force F_u	Final Deflection, $F_u.\delta$ (mm)
AB	7486	1000	14400	0	0.0000	1	0.00
AC	7486	750	14400	-5	-0.0348	0	0.00
CB	410	1000	120000	-17.5	-0.3557	-1.25	0.44
BD	7486	750	14400	5.5	0.0383	0.75	0.03
CD	7486	1000	14400	14	0.1299	1	0.13
CE	7486	750	14400	-15.5	-0.1078	-0.75	0.08
ED	410	1000	120000	-17.5	-0.3557	-1.25	0.44
DF	7486	750	14400	15.5	0.1078	0.75	0.08
					Total Deflection		1.21

942

943

Table 8 Deflection of Frame 1 at post-cracking (21kN)

Member	E (N/mm2)	Length (mm)	Area (mm2)	Force (kN)	Deflection, δ (mm)	Unit Force Fu	Final Deflection, Fu.δ (mm)
AB	7486	1000	14400	0	0.0000	1	0.00
AC	7486	750	14400	-5	-0.0348	0	0.00
CB	410	1000	12720	-26	-4.9854	-1.25	6.23
BD	7486	750	14400	10.6	0.0737	0.75	0.06
CD	7486	1000	14400	20.8	0.1930	1	0.19
CE	7486	750	14400	-20.6	-0.1433	-0.75	0.11
ED	410	1000	11160	-26	-5.6823	-1.25	7.10
DF	7486	750	14400	26.2	0.1823	0.75	0.14
					Total Deflection		13.83

Table 9 Deflection of Frame 2 at post-cracking (18kN)

Member	E (N/mm2)	Length (mm)	Area (mm2)	Force (kN)	Deflection, δ (mm)	Unit Force F_u	Final Deflection, $F_u.\delta$ (mm)
AB	7486	1000	14400	0	0.0000	1	0.0000
AC	7486	750	14400	-5	-0.0348	0	0.0000
CB	382	1000	12600	-22.5	-4.6746	-1.25	5.8433
BD	7486	750	14400	8.5	0.0591	0.75	0.0444
CD	7486	1000	14400	18	0.1670	1	0.1670
CE	7486	750	14400	18.5	0.1287	-0.75	-0.0965
ED	382	1000	14040	-22.5	-4.1952	-1.25	5.2440
DF	7486	750	14400	22	0.1531	0.75	0.1148
					Total Deflection		11.32

951 *Table 10 Deflection of Frame 3 at post-cracking (16kN)*

Member	E (N/mm2)	Length (mm)	Area (mm2)	Force (kN)	Deflection, δ (mm)	Unit Force F_u	Final Deflection, $F_u.\delta$ (mm)
AB	7486	1000	14400	0	0.0000	1	0.0000
AC	7486	750	14400	-5	-0.0348	0	0.0000
CB	382	1000	13440	-20	-3.8955	-1.25	4.8694
BD	7486	750	14400	7	0.0487	0.75	0.0365
CD	7486	1000	14400	16	0.1484	1	0.1484
CE	7486	750	14400	-17	-0.1183	-0.75	0.0887
ED	382	1000	13440	-20	-3.8955	-1.25	4.8694
DF	7486	750	14400	19	0.1322	0.75	0.0991
					Total Deflection		10.11

952

953

954 *Table 11 Deflection of Frame 4 at post-cracking (6kN)*

Member	E (N/mm2)	Length (mm)	Area (mm2)	Force (kN)	Deflection, δ (mm)	Unit Force F_u	Final Deflection, $F_u.\delta$ (mm)
AB	7486	1000	14400	0	0.0000	1	0.00
AC	7486	750	14400	-5	-0.0348	0	0.00
CB	210	1000	11760	-7.5	-3.0369	-1.25	3.80
BD	7486	750	14400	0.5	0.0035	0.75	0.00
CD	7486	1000	14400	6	0.0557	1	0.06
CE	7486	750	14400	-9.5	-0.0661	-0.75	0.05
ED	210	1000	11760	-7.5	-3.0369	-1.25	3.80
DF	7486	750	14400	4	0.0278	0.75	0.02
					Total Deflection		7.72

955
956

Figure 1

Click here to access/download;Figure;Figure 1.tif

Figure 2

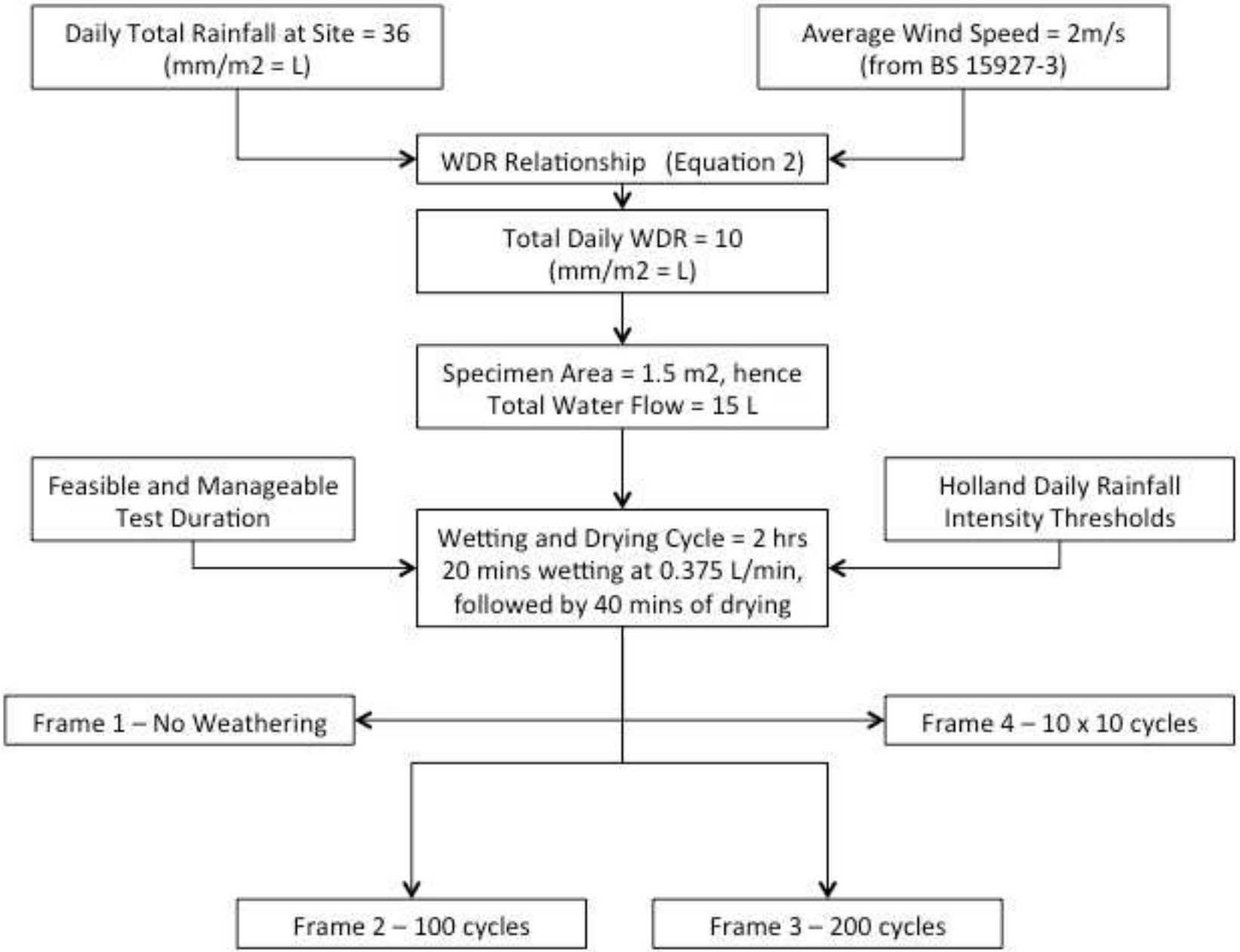

Figure 3

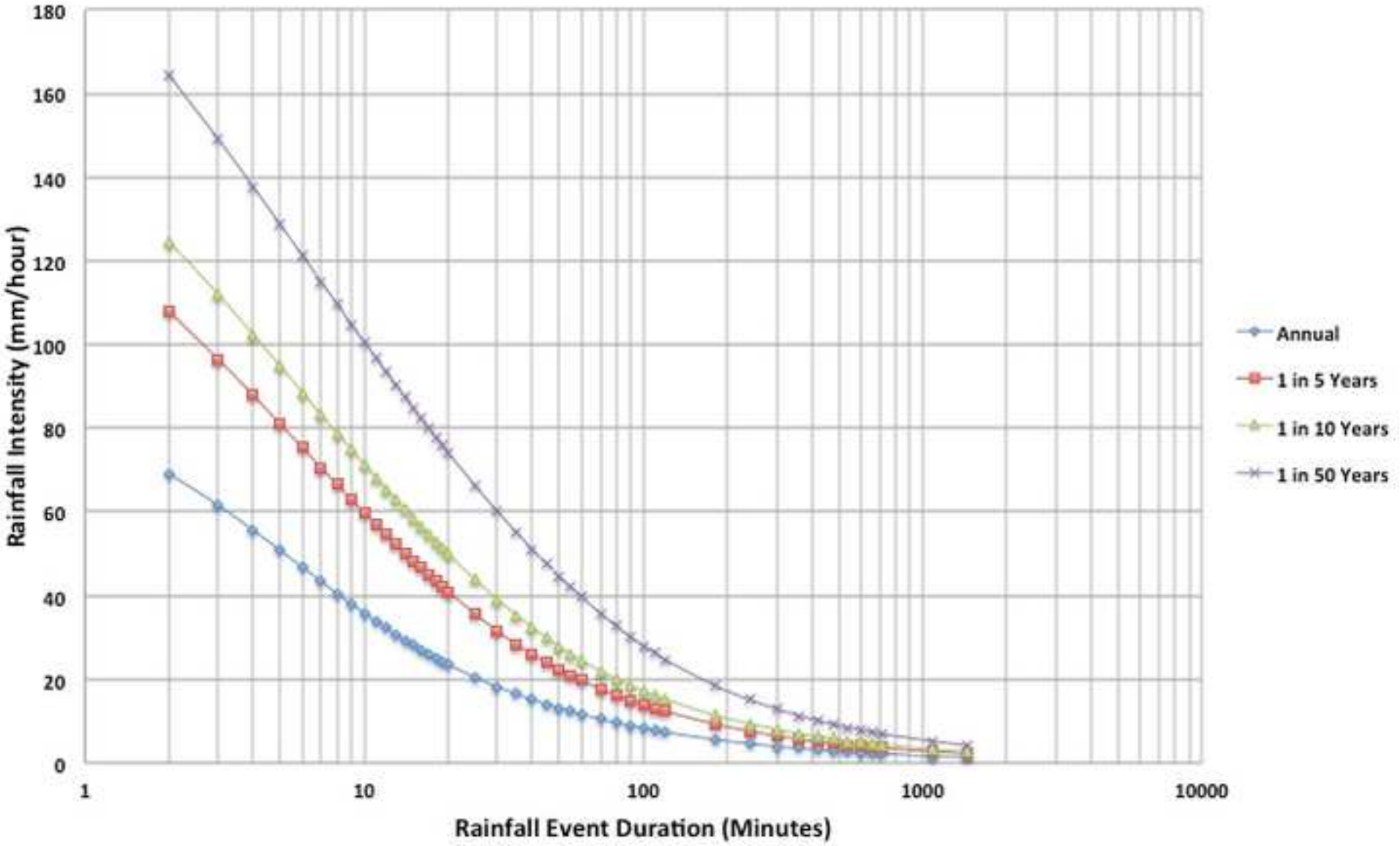

Figure 4

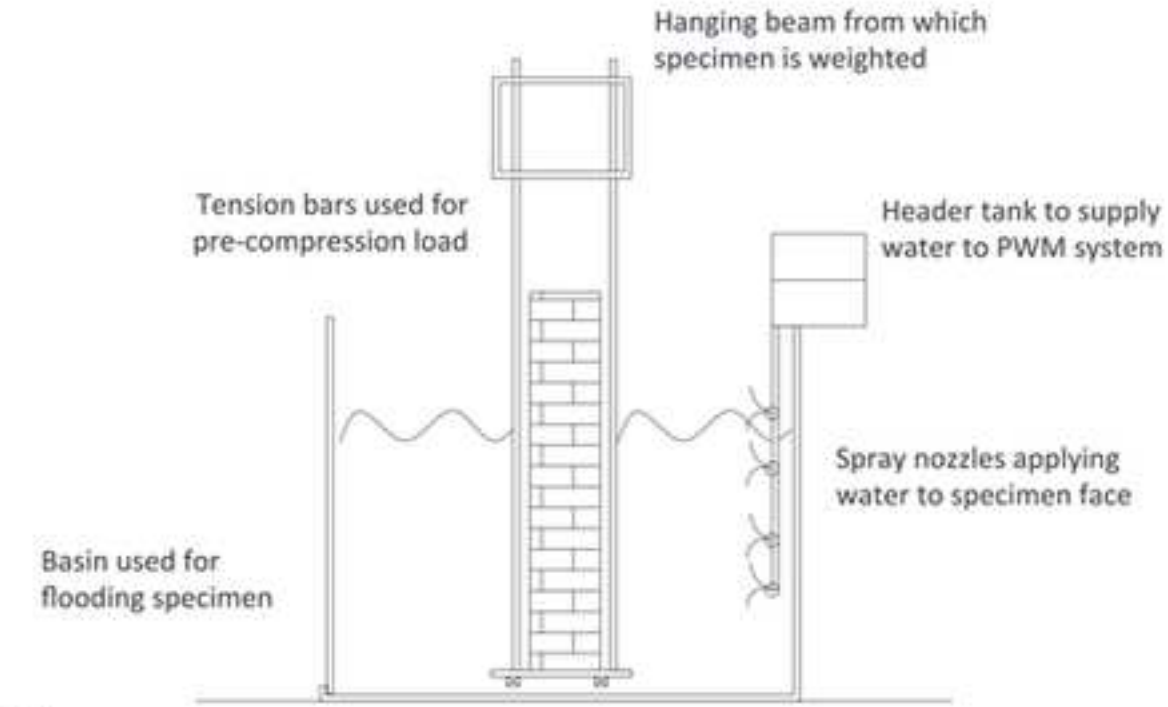

(a)

(b)

Figure 5

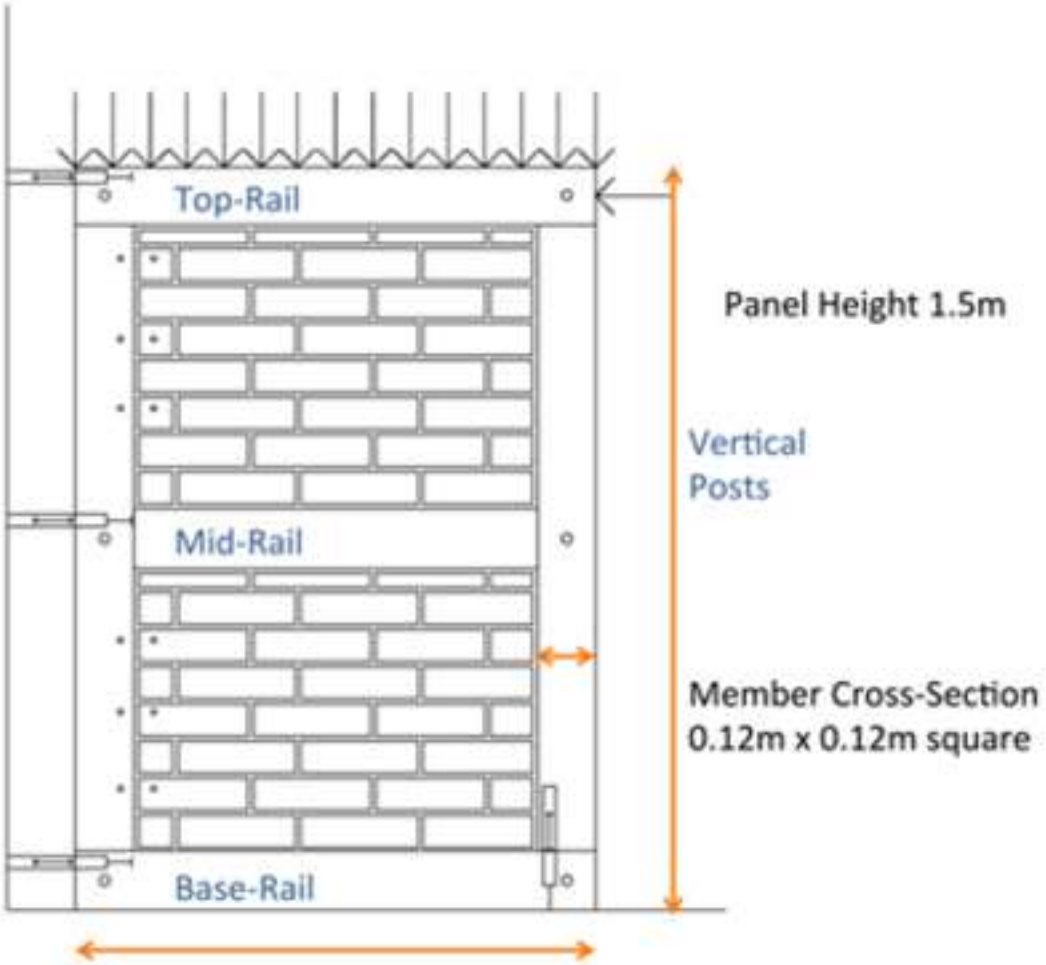

(a)

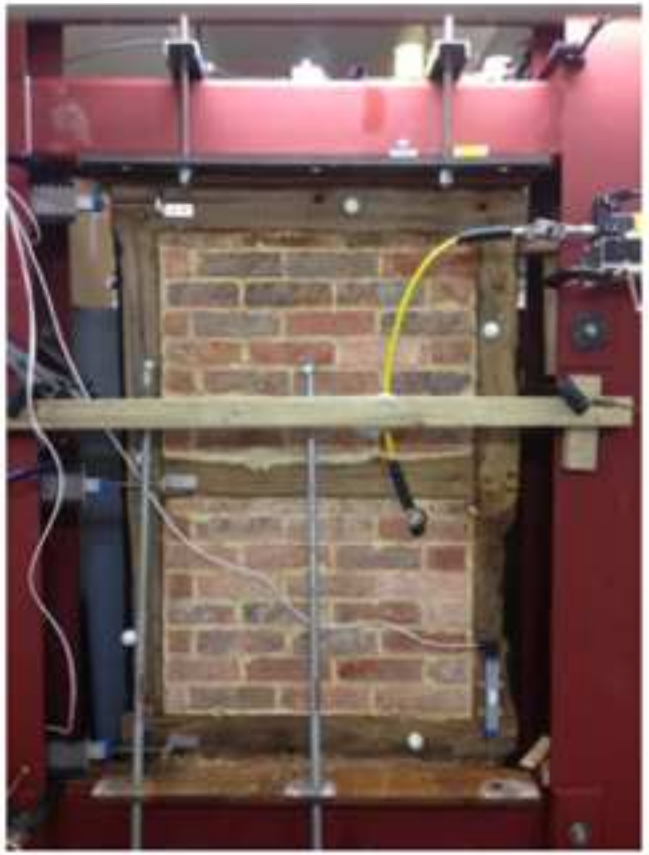

(b)

Figure 6

Click here to access/download;Figure;Figure 6.tif

Figure 7

Click here to access/download;Figure;Figure 7.tif

Figure 8

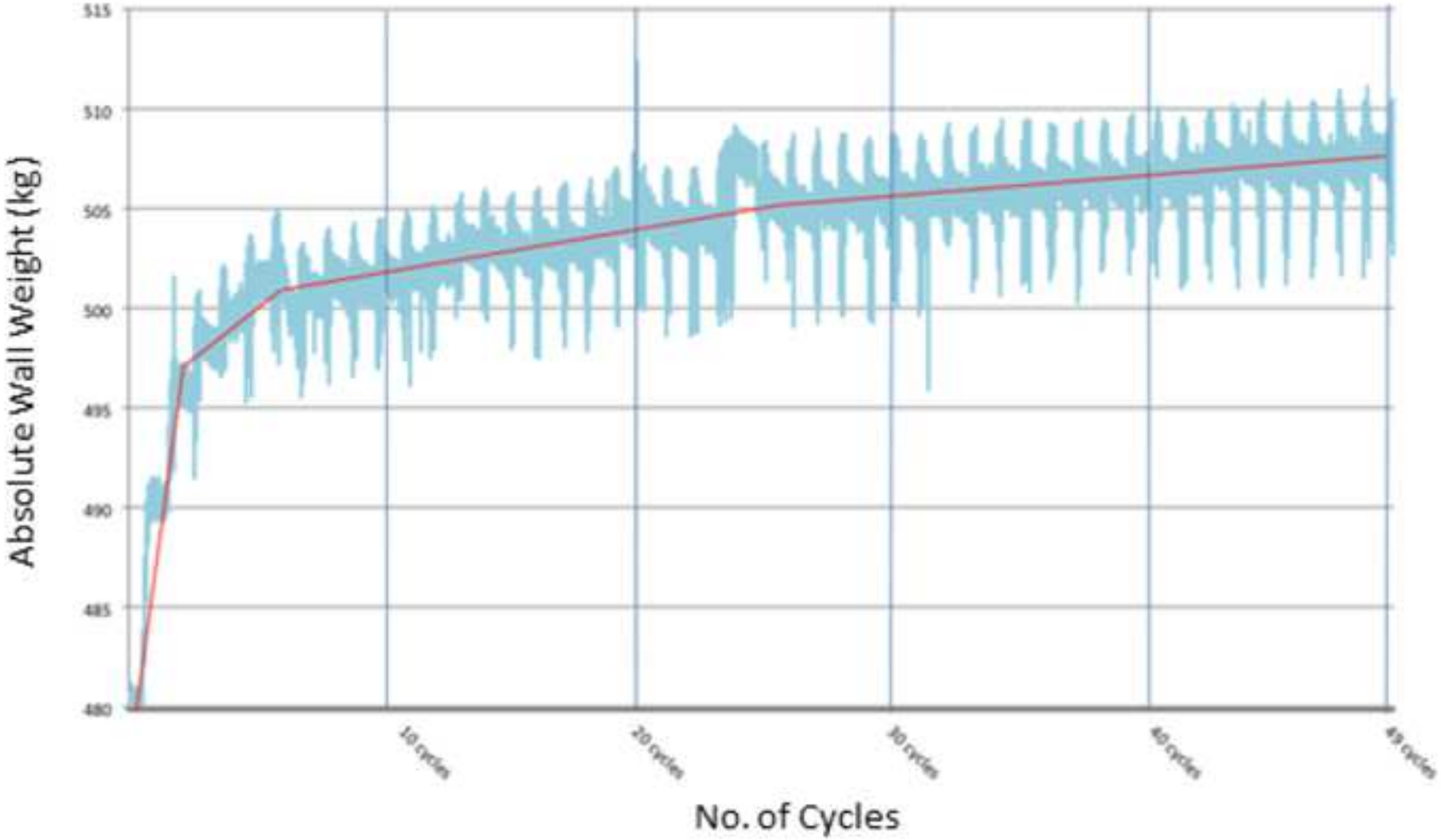

Figure 9

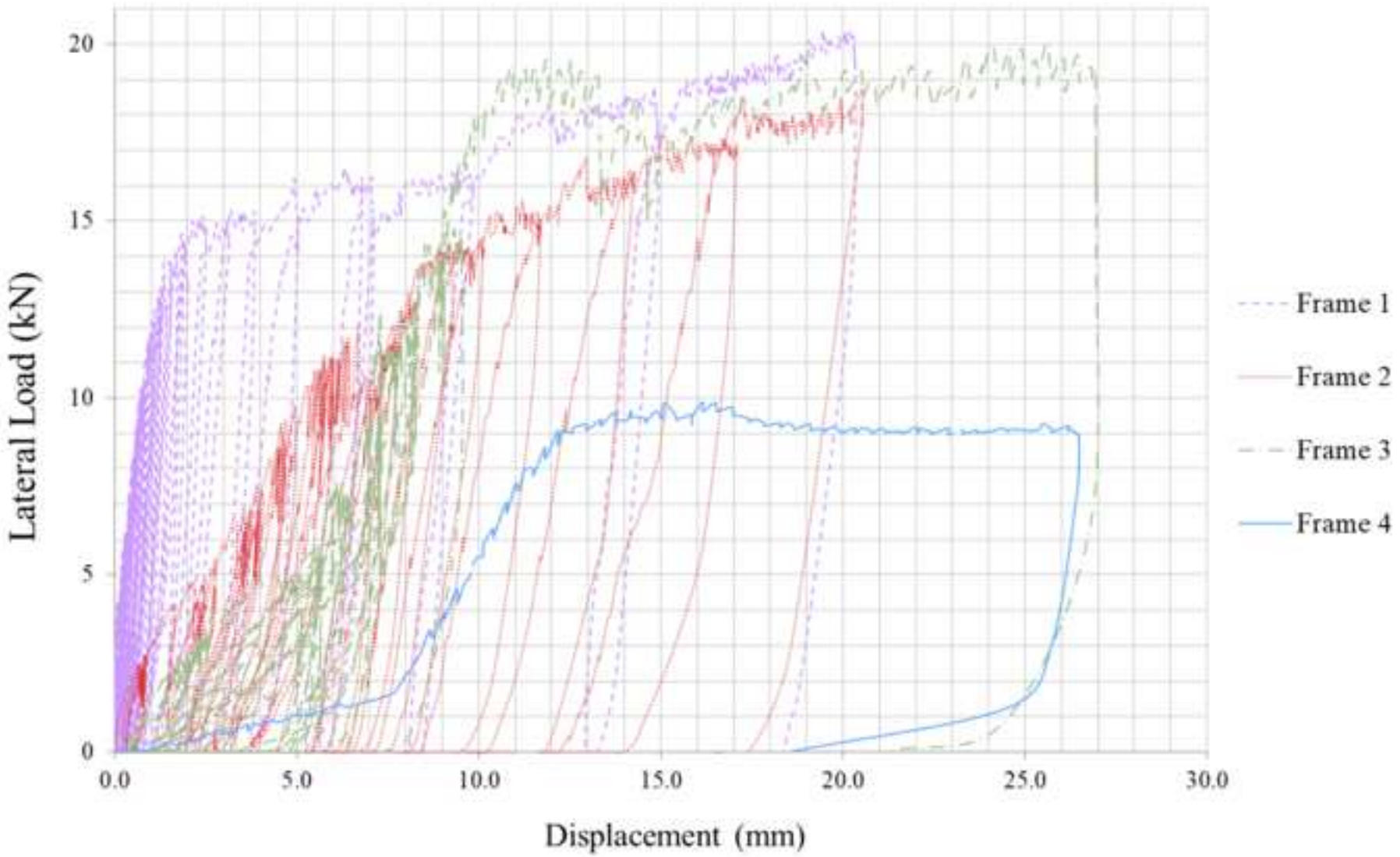

Figure 10

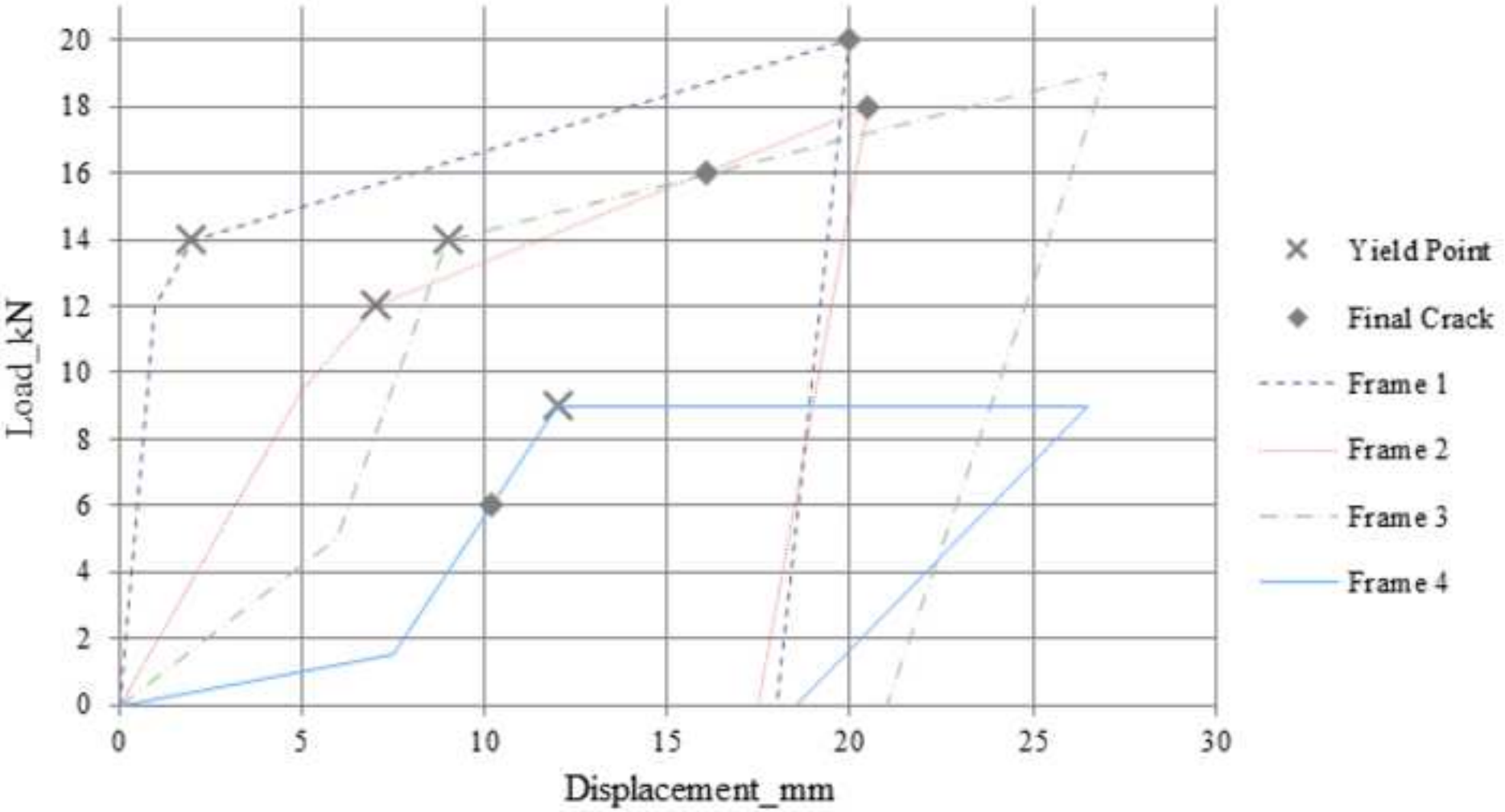

Figure 11

Click here to access/download;Figure;Figure 11.tif

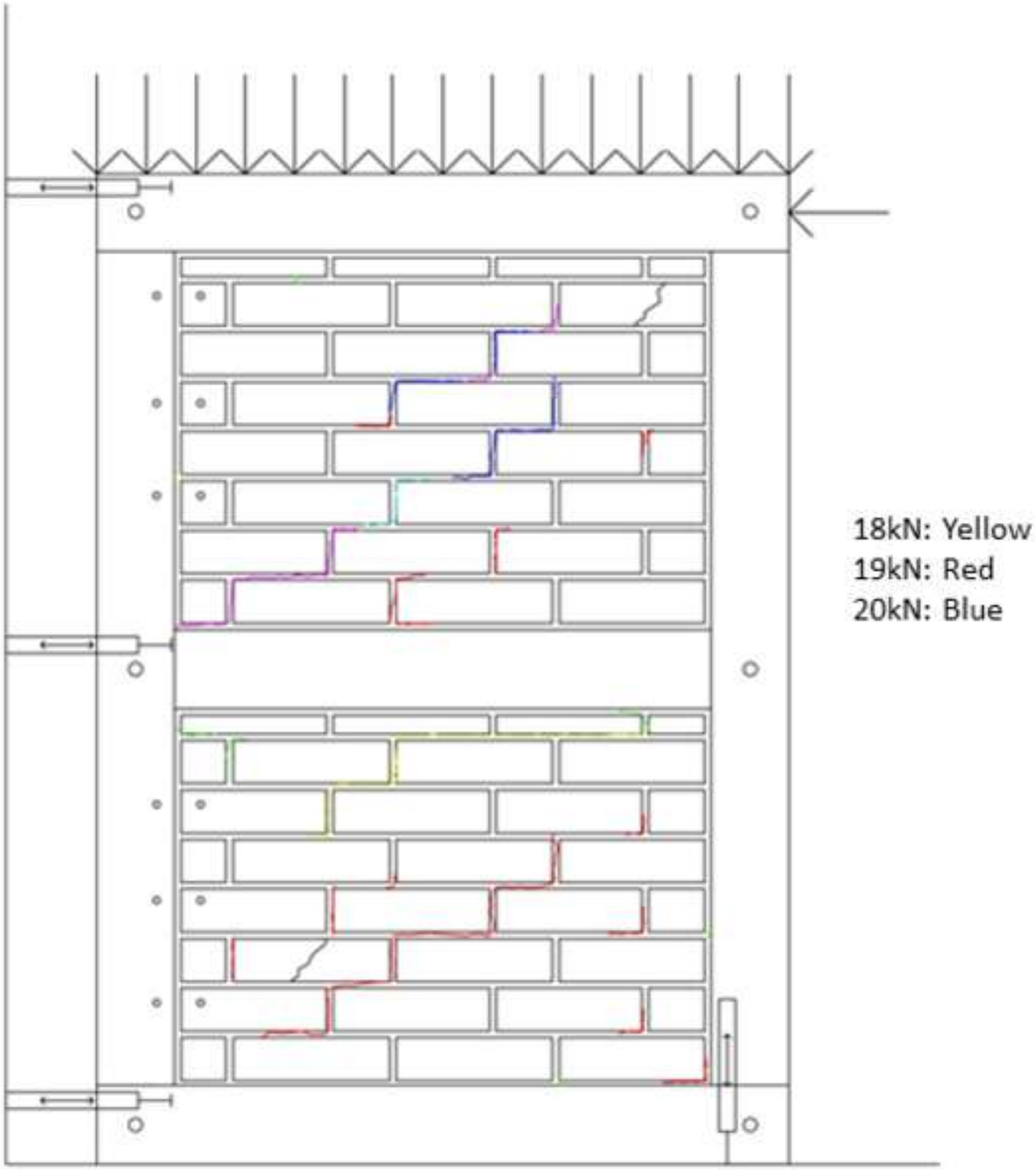

Figure 12

Click here to access/download;Figure;Figure 12.tif

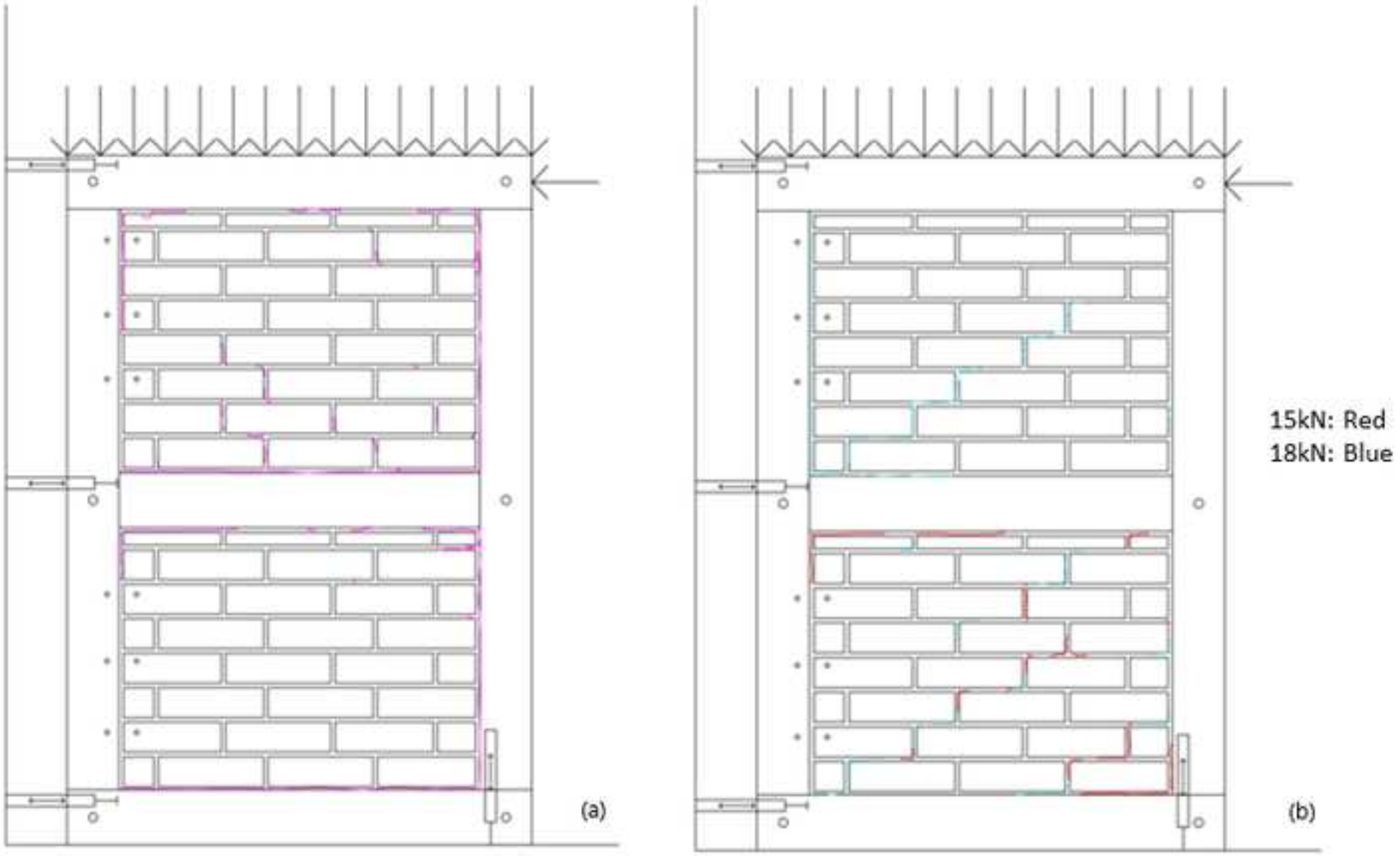

Figure 13

Click here to access/download;Figure;Figure 13.tif

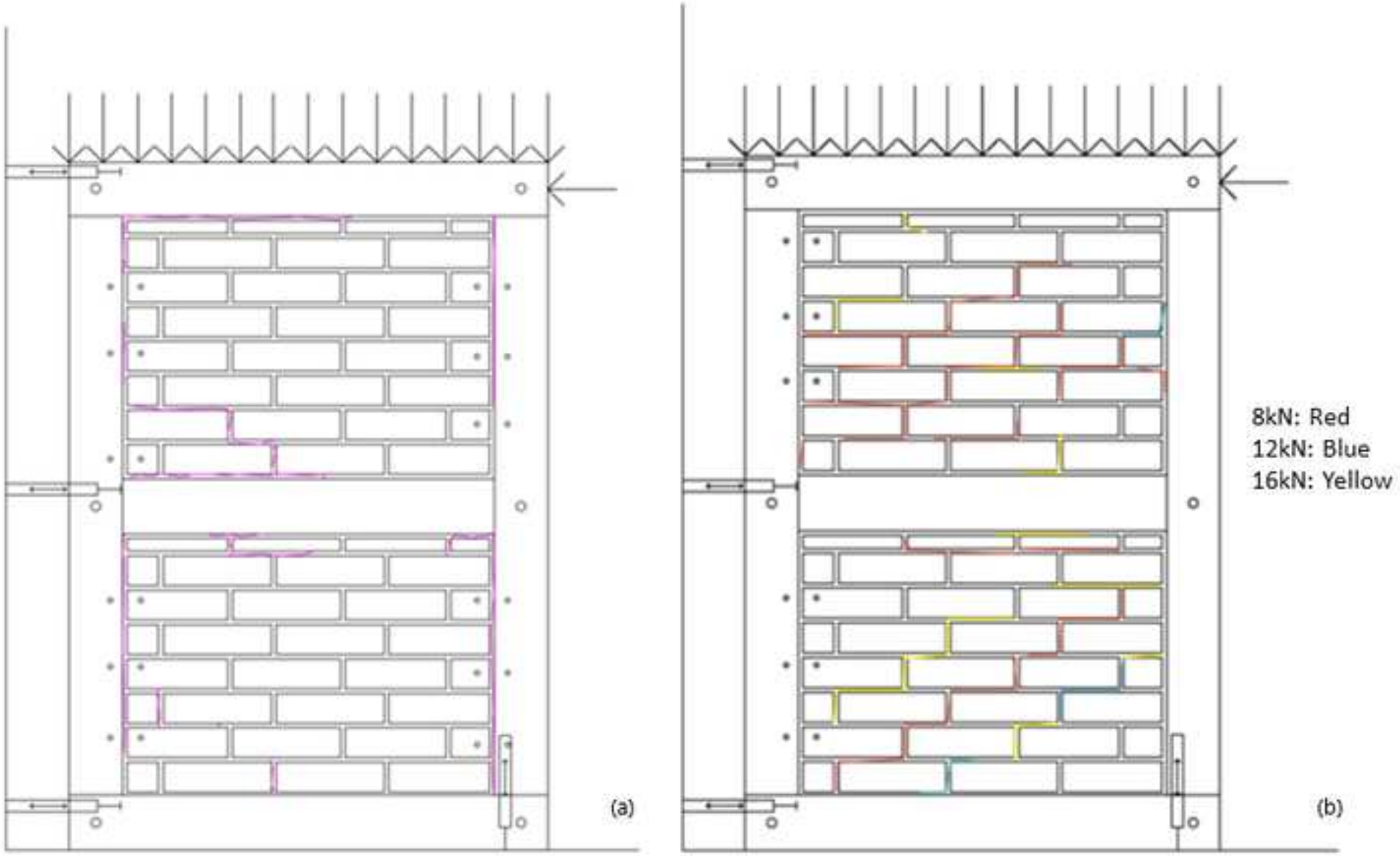

Figure 14

Click here to access/download;Figure;Figure 14.tif

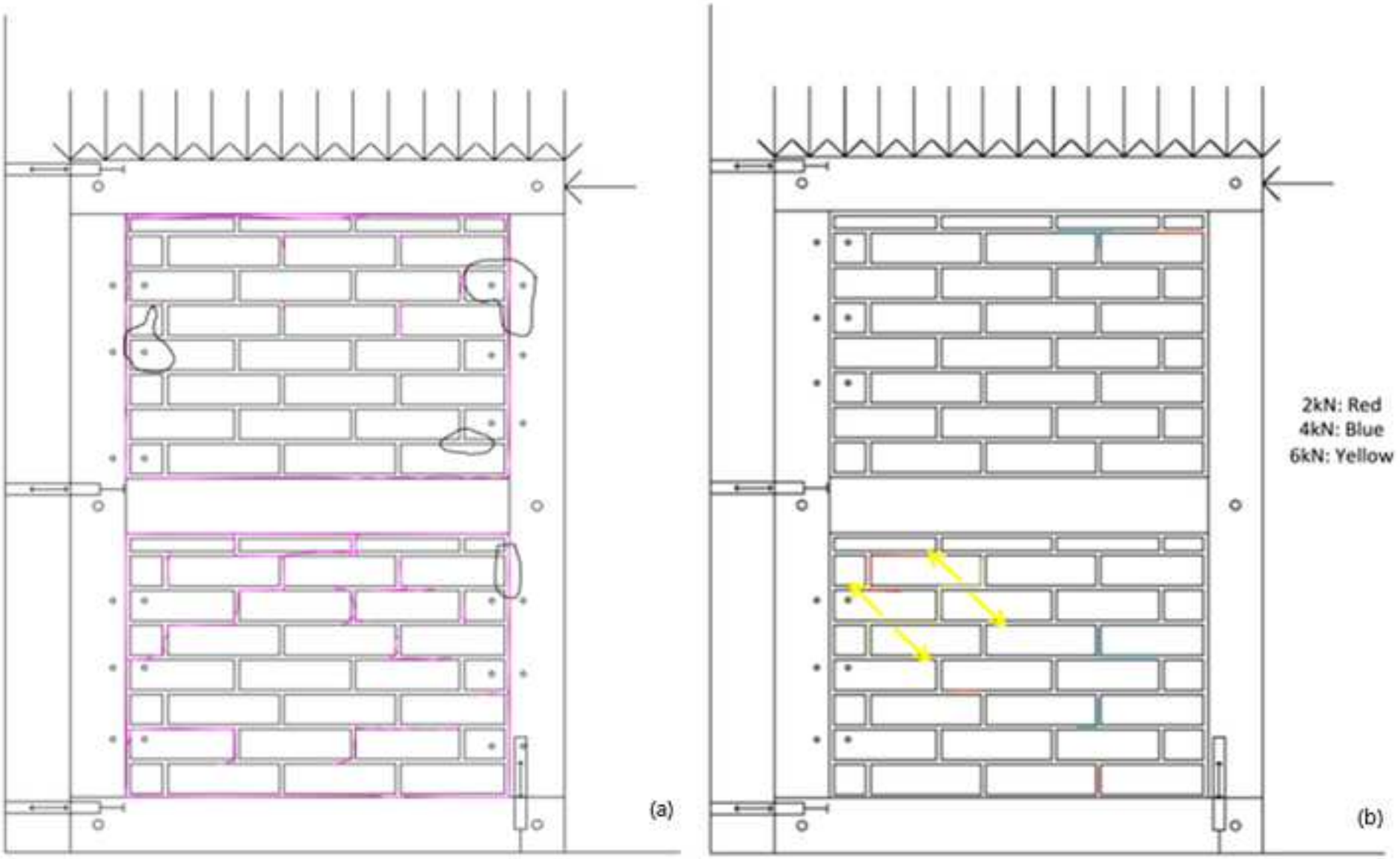

Figure 15

Click here to access/download;Figure;Figure 15.tif

Figure 16

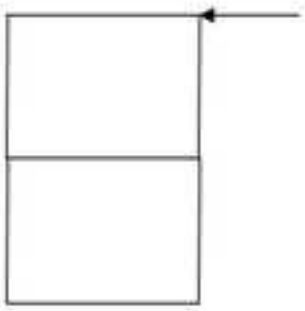

Frame Un-deformed

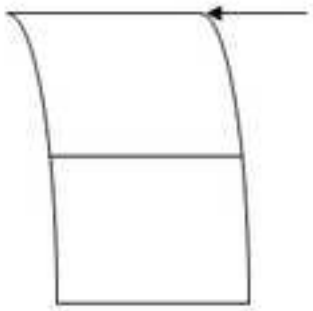

Frame in Elastic Bending Deformation

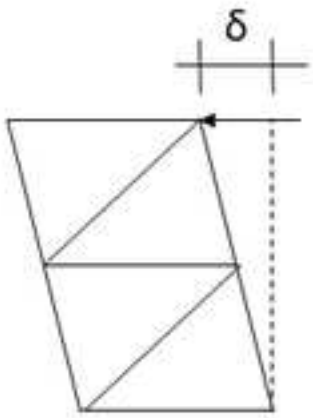

Frame in Post-Elastic Deformation

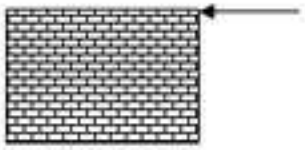

Masonry Un-deformed

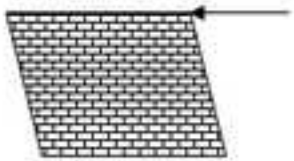

Masonry in Shear

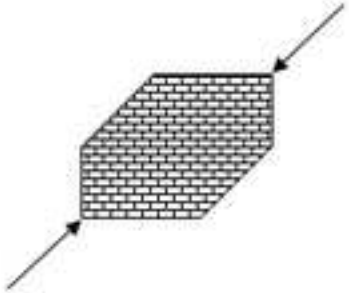

Masonry as Compression Strut

Figure 17

Click here to access/download;Figure;Figure 17.tif

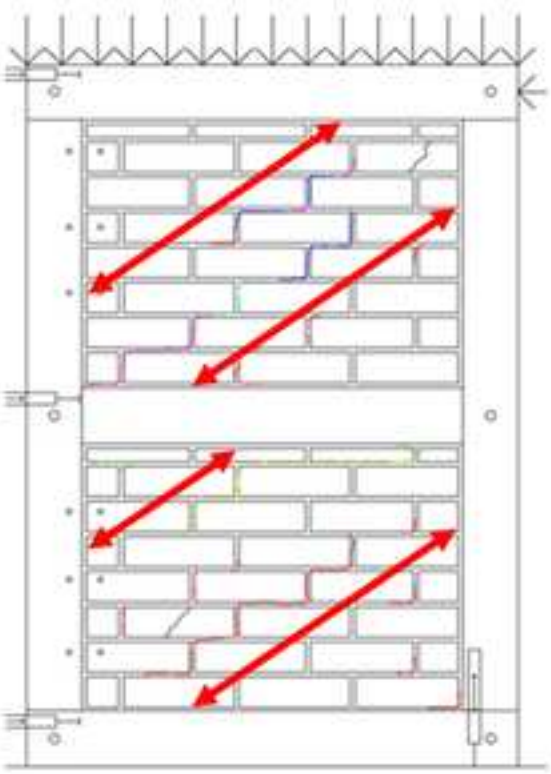

Frame 1

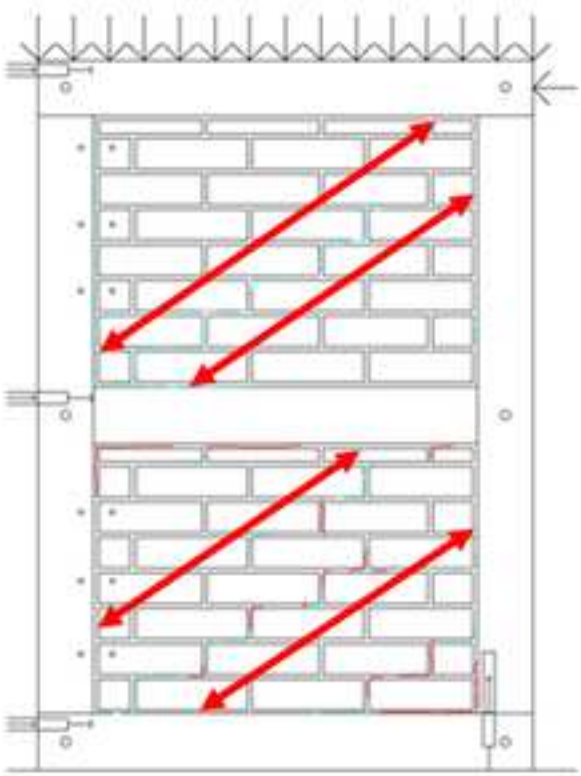

Frame 2

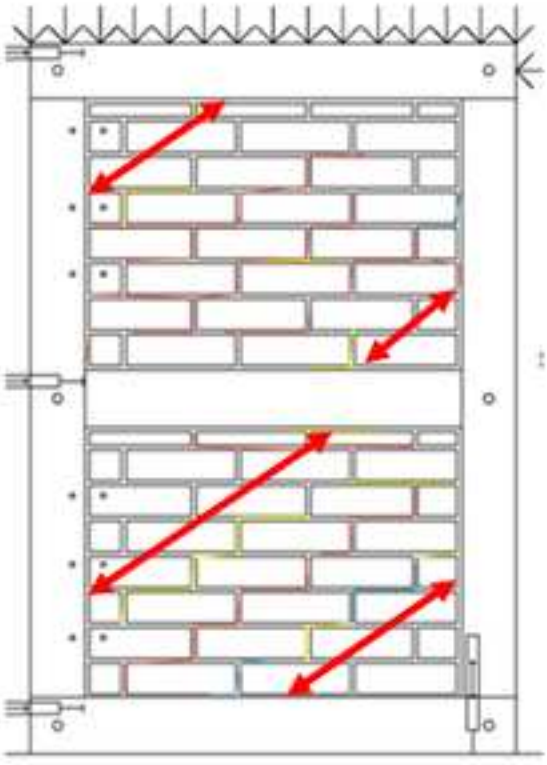

Frame 3

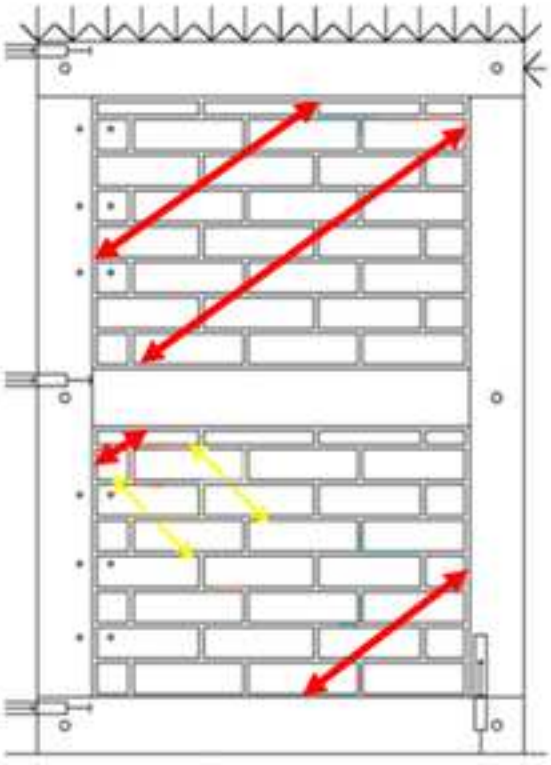

Frame 4

Figure 18

Click here to access/download;Figure;Figure 18.tif

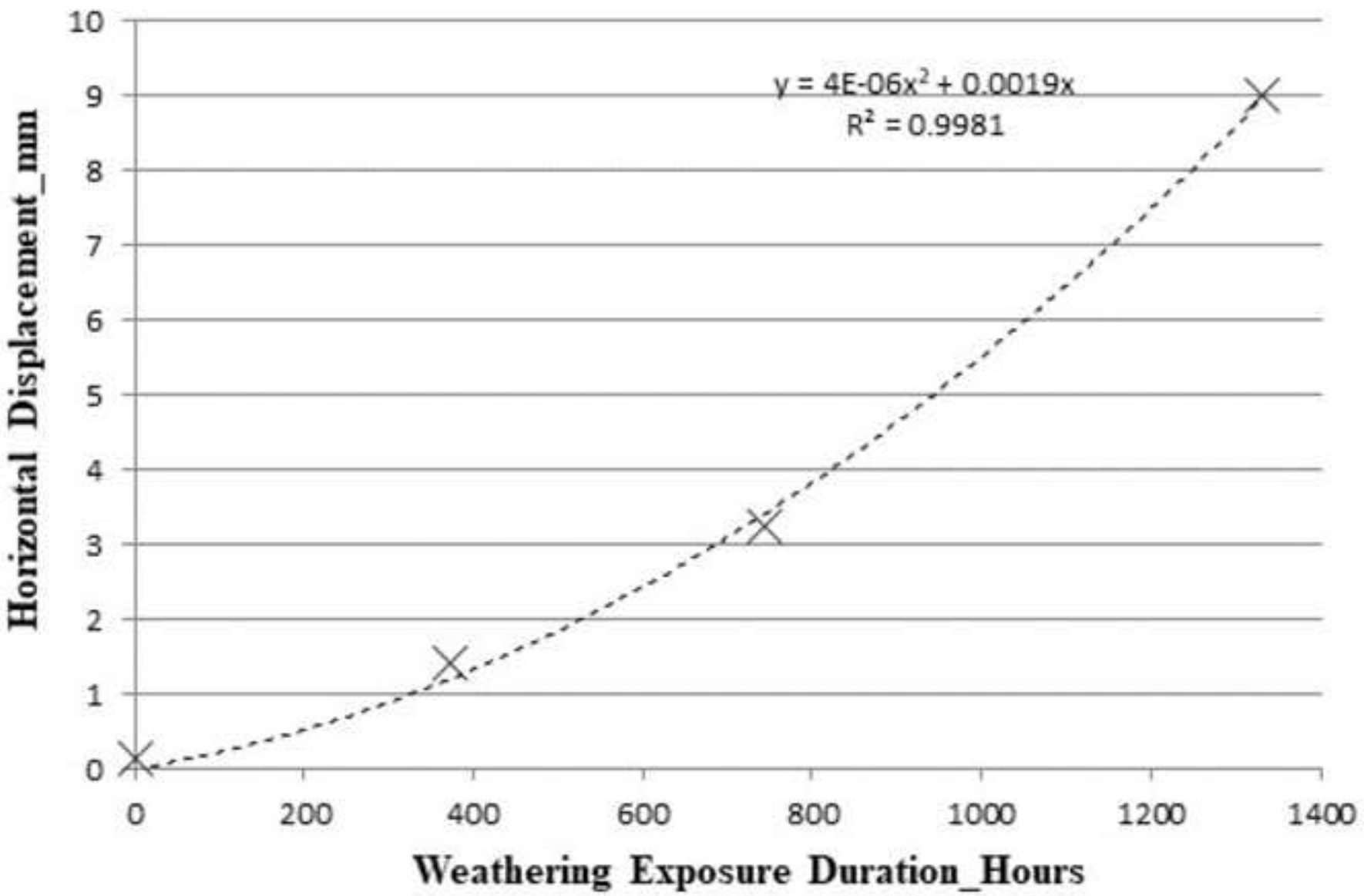

Figure 19

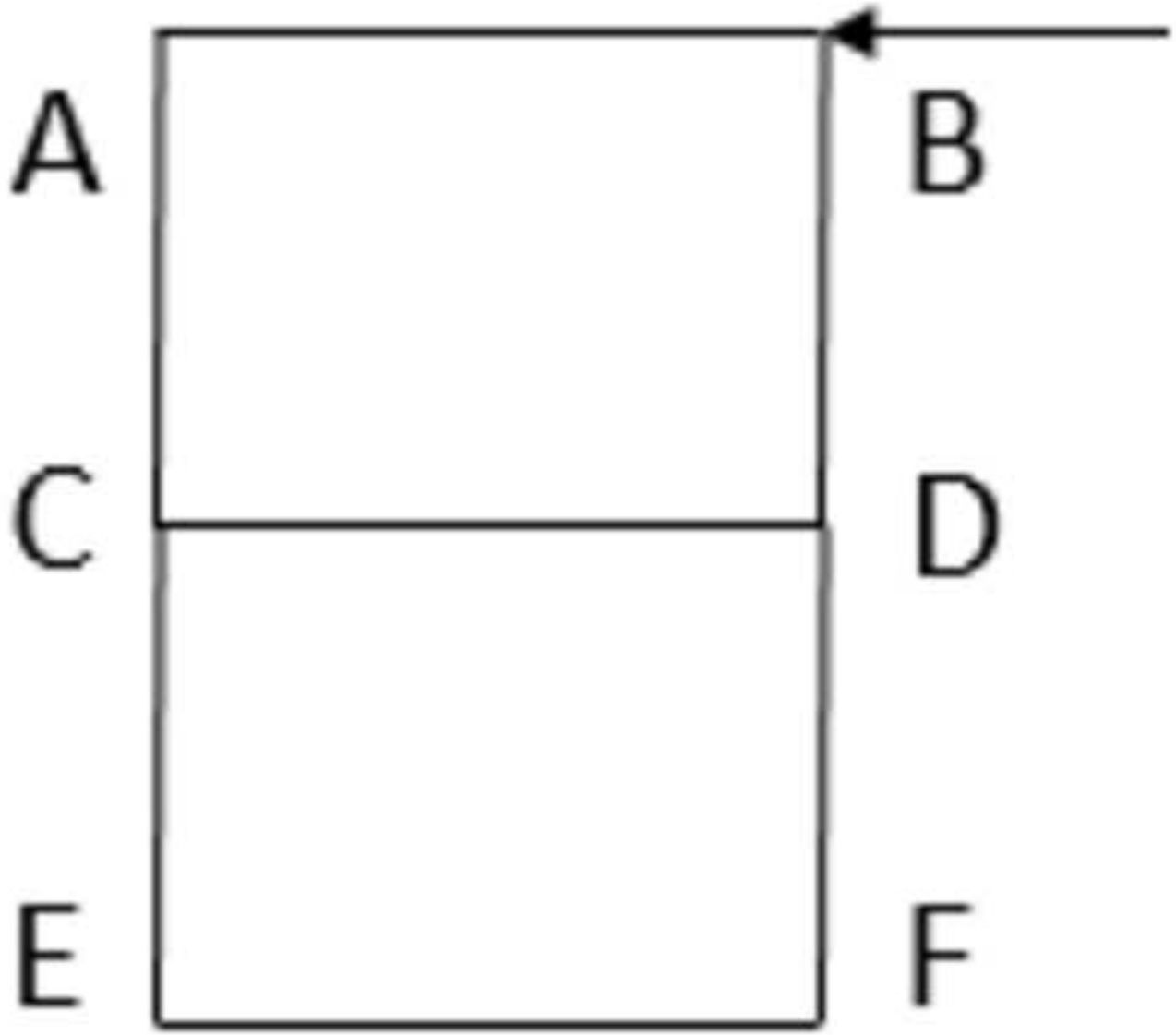

Figure 20

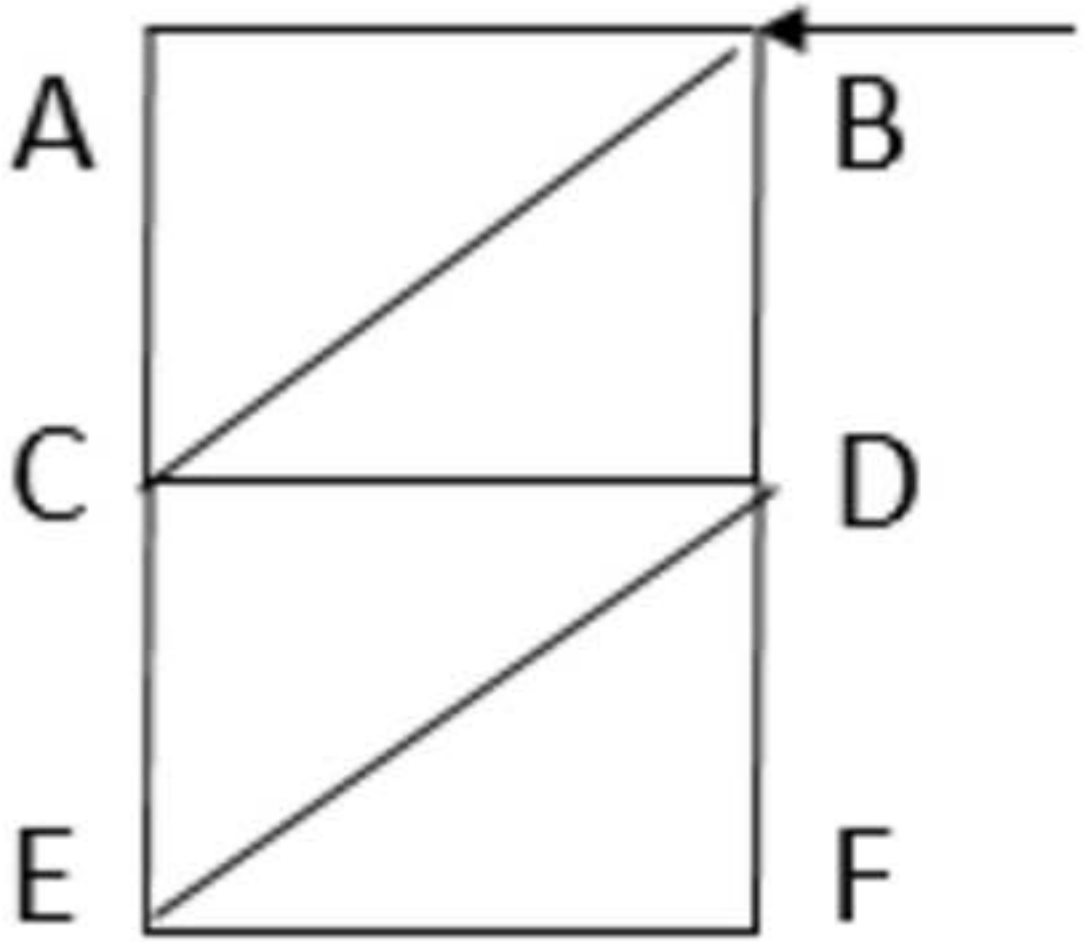

Figure Captions List

ASCE Authorship, Originality, and Copyright Transfer Agreement

Publication Title: ~~Structural Response~~ J. of the Perf. of Constr. Facil.

Manuscript Title: Structural Response of Masonry Infilled Timber Frames to Flood and Wind Driven Rain Exposure

Author(s) – **Names, postal addresses, and e-mail addresses of all authors**

Dr Victoria Stephenson
CEGE, UCL, Chadwick Building, Gower Street, London, WC1E 6BT
victoria.stephenson.12@ucl.ac.uk

Prof. Dina D'Ayala d.dayala@ucl.ac.uk
CEGE, UCL, Chadwick Building, Gower Street, London, WC1E 6BT

I. Authorship Responsibility

To protect the integrity of authorship, only people who have significantly contributed to the research or project and manuscript preparation shall be listed as coauthors. The corresponding author attests to the fact that anyone named as a coauthor has seen the final version of the manuscript and has agreed to its submission for publication. Deceased persons who meet the criteria for coauthorship shall be included, with a footnote reporting date of death. No fictitious name shall be given as an author or coauthor. An author who submits a manuscript for publication accepts responsibility for having properly included all, and only, qualified coauthors.

I, the corresponding author, confirm that the authors listed on the manuscript are aware of their authorship status and qualify to be authors on the manuscript according to the guidelines above.

VICTORIA STEPHENSON — Print Name

Signature

14/09/18 — Date

II. Originality of Content

ASCE respects the copyright ownership of other publishers. ASCE requires authors to obtain permission from the copyright holder to reproduce any material that (1) they did not create themselves and/or (2) has been previously published, to include the authors' own work for which copyright was transferred to an entity other than ASCE. Each author has a responsibility to identify materials that require permission by including a citation in the figure or table caption or in extracted text. Materials re-used from an open access repository or in the public domain must still include a citation and URL, if applicable. At the time of submission, authors must provide verification that the copyright owner will permit re-use by a commercial publisher in print and electronic forms with worldwide distribution. For Conference Proceeding manuscripts submitted through the ASCE online submission system, authors are asked to verify that they have permission to re-use content where applicable. Written permissions are not required at submission but must be provided to ASCE if requested. Regardless of acceptance, no manuscript or part of a manuscript will be published by ASCE without proper verification of all necessary permissions to re-use. ASCE accepts no responsibility for verifying permissions provided by the author. Any breach of copyright will result in retraction of the published manuscript.

I, the corresponding author, confirm that all of the content, figures (drawings, charts, photographs, etc.), and tables in the submitted work are either original work created by the authors listed on the manuscript or work for which permission to re-use has been obtained from the creator. For any figures, tables, or text blocks exceeding 100 words from a journal article or 500 words from a book, written permission from the copyright holder has been obtained and supplied with the submission.

VICTORIA STEPHENSON — Print name

Signature

14/09/18 — Date

III. Copyright Transfer

ASCE requires that authors or their agents assign copyright to ASCE for all original content published by ASCE. The author(s) warrant(s) that the above-cited manuscript is the original work of the author(s) and has never been published in its present form.

The undersigned, with the consent of all authors, hereby transfers, to the extent that there is copyright to be transferred, the exclusive copyright interest in the above-cited manuscript (subsequently called the "work") in this and all subsequent editions of the work (to include closures and errata), and in derivatives, translations, or ancillaries, in English and in foreign translations, in all formats and media of expression now known or later developed, including electronic, to the American Society of Civil Engineers subject to the following:

- The undersigned author and all coauthors retain the right to revise, adapt, prepare derivative works, present orally, or distribute the work, provided that all such use is for the personal noncommercial benefit of the author(s) and is consistent with any prior contractual agreement between the undersigned and/or coauthors and their employer(s).
- No proprietary right other than copyright is claimed by ASCE.
- If the manuscript is not accepted for publication by ASCE or is withdrawn by the author prior to publication (online or in print), this transfer will be null and void.
- Authors may post a PDF of the ASCE-published version of their work on their employers' ***Intranet*** with password protection. The following statement must appear with the work: "This material may be downloaded for personal use only. Any other use requires prior permission of the American Society of Civil Engineers."
- Authors may post the ***final draft*** of their work on open, unrestricted Internet sites or deposit it in an institutional repository when the draft contains a link to the published version at www.ascelibrary.org. "Final draft" means the version submitted to ASCE after peer review and prior to copyediting or other ASCE production activities; it does not include the copyedited version, the page proof, a PDF, or full-text HTML of the published version.

Exceptions to the Copyright Transfer policy exist in the following circumstances. Check the appropriate box below to indicate whether you are claiming an exception:

☐ **U.S. GOVERNMENT EMPLOYEES:** Work prepared by U.S. Government employees in their official capacities is not subject to copyright in the United States. Such authors must place their work in the public domain, meaning that it can be freely copied, republished, or redistributed. In order for the work to be placed in the public domain, ALL AUTHORS must be official U.S. Government employees. If at least one author is not a U.S. Government employee, copyright must be transferred to ASCE by that author.

☐ **CROWN GOVERNMENT COPYRIGHT:** Whereby a work is prepared by officers of the Crown Government in their official capacities, the Crown Government reserves its own copyright under national law. If ALL AUTHORS on the manuscript are Crown Government employees, copyright cannot be transferred to ASCE; however, ASCE is given the following nonexclusive rights. (1) to use, print, and/or publish in any language and any format, print and electronic, the above-mentioned work or any part thereof, provided that the name of the author and the Crown Government affiliation is clearly indicated; (2) to grant the same rights to others to print or publish the work, and (3) to collect royalty fees. ALL AUTHORS must be official Crown Government employees in order to claim this exemption in its entirety. If at least one author is not a Crown Government employee, copyright must be transferred to ASCE by that author.

☐ **WORK-FOR-HIRE:** Privately employed authors who have prepared works in their official capacity as employees must also transfer copyright to ASCE, however, their employer retains the rights to revise, adapt, prepare derivative works, publish, reprint, reproduce, and distribute the work provided that such use is for the promotion of its business enterprise and does not imply the endorsement of ASCE. In this instance, an authorized agent from the authors' employer must sign the form below.

☐ **U.S. GOVERNMENT CONTRACTORS:** Work prepared by authors under a contract for the U.S. Government (e.g., U.S. Government labs) may or may not be subject to copyright transfer. Authors must refer to their contractor agreement. For works that qualify as U.S. Government works by a contractor, ASCE acknowledges that the U.S. Government retains a nonexclusive, paid-up, irrevocable, worldwide license to publish or reproduce this work for U.S. Government purposes only. This policy DOES NOT apply to work created with U.S. Government grants.

I, the corresponding author, acting with consent of all authors listed on the manuscript, hereby transfer copyright or claim exemption to transfer copyright of the work as indicated above to the American Society of Civil Engineers.

VICTORIA STEPHENSON

Print Name of Author or Agent

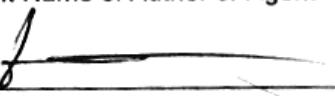

14/09/18

Signature of Author of Agent Date

More information regarding the policies of ASCE can be found at http://www.asce.org/authorsandeditors

Response to Reviewers' comments:

The authors would like to thank the reviewers for their thorough assessment of the manuscript, and are pleased to hear it was generally well received. Please see below responses to specific comments:

Reviewer #1:

(1) The experimental test conditions were derived from climate hazard data which seems not to consider the impacts of future climate changes. Would it be possible for the authors to discuss how to interpret the findings of the testing, considering the climate changes?

As the reviewer states the test conditions do not incorporate any specific climate change increment or factor, rather the test was designed to provide correlation of loss with weathering severity. Work elsewhere in the Parnassus project sought to measure climate change driven impacts, (Smith, A., Stephenson, V., Bates, P., D'Ayala, D., Freer, J. Projecting future flood risk: Highlighting the impacts on high value buildings. 8th Alex. von Humboldt Int. Conf., Cusco, Peru, Nov. 12th-16th, 2013) however the results were not sufficiently robust for use in the testing programme reported on here. It is difficult therefore to discuss in any quantitative terms the findings of the testing in relation to climate change measures, rather the fact that a positive correlation exists highlights that any climatic change which leads to increasing severity of conditions will potentially lead to greater losses. Statements are included in lines 198 – 201 and 629 - 631 to this effect.

(2) In the line of 189, the wetting and drying cycle parameters were determined as "40 minutes of wetting" and "2 hr and 20 min. period of drying". It is not quite clear how to determine these parameters. If the information from Figure 3 was used to determine these parameter, the authors need discuss how the climate changes influence the wetting and drying cycles since the data in Figure 3 were published in 1960.

Thanks to the reviewer for highlighting a mistake in the text; the reference to the figure on line 172 should state "Figure 2". Figure 2 describes the stages in calculating the above mentioned parameters. The exact values derive from a 30-year dataset from the period 1981 – 2011, so a current precipitation datum. The data produced in 1960 is only considered in relation to the intensity thresholds used, and to the author's knowledge there is no more recent data suitable for this purpose. Changes are made in the text (lines 175 - 182) to clarify these details.

(3) The authors need explain all parameters included in Equation 3 in the main body of the manuscript, although they were explained in the Appendix A.

Text has been added (lines 514 - 519) in the main body of the manuscript to reflect this request.

(4) A sketch for HMITF should be included in Appendix A with all nodes (A, B, ...F) marked in the drawing, to help readers interpret the equations of slope deflection and diagonal strut assessments used for elastic phase and post crack phase evaluations respectively.

A figure has been added to the Appendix (Figure A1).

(5) The authors evaluated the vulnerability of the HMITF subject to wind loading using a deterministic approach. Would it be possible for the authors to discuss how to use the findings of this work to inform future structural risk assessments?

As this is a first step in work towards better understanding of the structural performance of these types of structures specifically to wind driven rain, the authors feel that the simplicity afforded by a deterministic methodology is important to ensure the quality of the work. We do acknowledge however that a critical next step in ensuring this type of analysis is incorporated into risk assessment work, is to repeat the assessment with probabilistic input data. Text to this effect has been added to the concluding statement (lines 674 - 684).

Reviewer #3:

1. A bespoke test rig was introduced, however, no detailed photo of Wind Driven Rain and Flood Test Rig is presented in the paper.

   A photo has been added to Figure 4.

2. It is not clear whether the structural test are conducted under the weathering conditions, therefore, more detailed description of the test rigs are needed.
   Text has been added (lines 266 – 268) to the initial description of the structural test to clarify that this was a separate test, carried out in a different test rig to the weathering tests.

3. Different structural forms of the Masonry Infilled Timber Frames should be investigated to make the conclusion more convincing.
   This is agreed as a key next step, and text has been added (lines 665 - 669 and 678 - 679) to the concluding statement to acknowledge that the tests so far are only applicable to the specific structural form used in the test specimens.

Reviewer #2:

Lines 201-202
Was Frame 3 subjected to 100 cycles and 100 year return flood, followed by another 100 cycles and another 100 year return flood?
Yes, this is correct.

Lines 354-356
Regarding the modules of elasticity, the authors should list the value from (Aras & Altay, 2015) and provide the percentage difference between the published value and their tested values. Is the empirical data for the same time period and type of mortar?
Table 1 and the preceding paragraph (lines 359 - 363) has been updated to reflect this comment. Two comparative empirical values of modulus of elasticity (E) have been provided, from studies of 18th and 19th century structures. The figures highlight that values of E can be highly variable this has additionally been commented on in the text.

Lines 381-386 Table 2
If Frame 3 was subjected to the exact same loading as Frame 2, and then repeated a second time, how does one explain the infill detachment being less than Frame 2? Shouldn't it have been comparable after the first set of loading, and gotten worse after it was repeated? In line 394 the author says "… a positive correlation exists… is not proportional to the number of weathering cycles…" and discusses some of the parameters, but it does not seem to indicate a positive correlation. More explanation is needed.
Thanks to the reviewer for highlighting this discrepancy, it is correct that a positive correlation does not exist and the text has been altered to reflect this fact. The parameters currently mentioned in the text (material variability) remain the author's opinion on the reasoning behind the non-linearity, and as such modified text (lines 395 - 399) in the manuscript reflects this.

Lines 458-463
Figure 11 shows structural cracks in Frame 1 (control specimen) but no cracks formed in Frame 2. Is that correct? This should be discussed.
Figure 12 shows the structural crack pattern for Frame 2 on the right hand side.

Line 525
The various used in equation 3 should be defined.
Text has been added to the main body of the manuscript to reflect this request (lines 514 - 519).

Line 660
"buildings" is misspelled.
This has now been corrected in the text.

Line 685
There should be a figure labeling points A, B, C and D
A figure has been added to the Appendix (Figure A2)